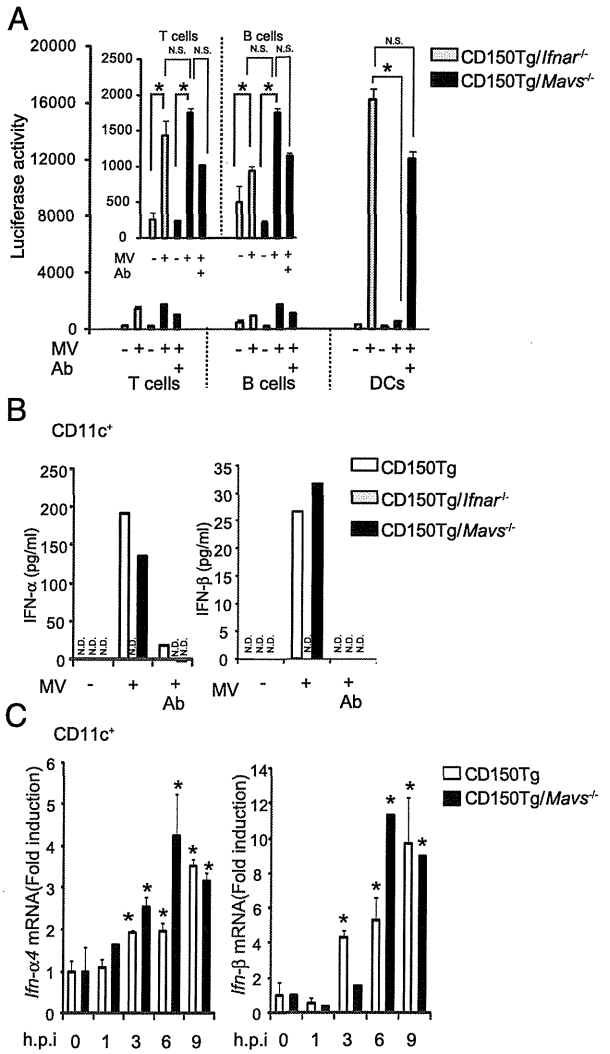

FIGURE 3. CD11c$^+$ DCs mainly produced type I IFN during MV infection in vitro. (**A**) T cells, B cells, and DCs were isolated from CD150Tg/*Ifnar*$^{-/-}$ and CD150Tg/*Mavs*$^{-/-}$ splenocytes, using MACS beads. Cells were treated with or without 10 μg/ml of anti-IFNAR Ab, then infected with mock or MV-luciferase at an MOI of 0.25. At 24 h post infection, luciferase activity was measured. Data are means ± SD of three independent samples. *$p < 0.05$. (**B**) CD11c$^+$ cells were prepared from splenocytes of CD150Tg, CD150Tg/*Ifnar*$^{-/-}$, and CD150Tg/*Mavs*$^{-/-}$ mice, using MACS beads. IFN-α and IFN-β protein production in culture supernatant of MV-infected cells (MOI = 0.25) was measured by ELISA. One of two experiments is shown. (**C**) CD11c$^+$ DCs were infected with MV (MOI of 0.25) for the indicated times, and type I IFN expression was determined by real-time PCR. Data are means ± SD of three independent samples. *A *t* test between 0 h.p.i. and the indicated time in respective mouse lines is $p < 0.05$. N.D., Not detected.

produced type I IFN (Fig. 4B, 4D) and were not permissive to MV (Fig. 4A, 4C). The resistance to MV infection was abolished by neutralizing type I IFNR with anti-IFNAR Ab (Fig. 4A, 4C). These data indicate that, like CD11c$^+$ DCs, CD150Tg/*Mavs*$^{-/-}$ pDCs and cDCs were barely permissive to MV because of the type I IFN production.

For more detailed study on the type I IFN-producing subsets, we further separated cDCs into CD8α$^+$, CD4$^+$, and DN DCs, using MACS beads. The purity of these subsets was > 90% (data not shown). *Ifn-β* mRNA was not induced in CD150Tg/*Mavs*$^{-/-}$ CD8α$^+$ DCs or DN DCs in response to MV infection (Fig. 5A, 5B). However, MV infection induced expression of *Ifn-β* mRNA in CD4$^+$ DCs from CD150Tg/*Mavs*$^{-/-}$ mice (Fig. 5C). Different from CD150Tg/*Mavs*$^{-/-}$ DCs, CD150Tg CD8α$^+$ and DN DCs expressed *Ifn-β* mRNA in response to MV infection (Fig. 5A, 5B). These data indicate that the expression of *Ifn-β* mRNA induced by MV infection is MAVS dependent in CD8α$^+$ DCs and DNs, but MAVS independent in CD4$^+$ DCs.

The MyD88-dependent pathway is essential for MV-induced type I IFN production in pDCs and CD4$^+$ DCs under MAVS deficiency

Next, we tried to identify the signaling pathway involved in type I IFN induction during MV infection. pDCs and CD4$^+$ DCs express TLR7 as a sensor for single-stranded RNA (34, 35). Recognition of single-stranded RNA through the TLR7-MyD88 pathway induces type I IFN expression in human and mouse pDCs (36–38). Therefore, we examined whether the TLR7-MyD88 pathway participated in the host defense during MV infection in mouse DCs. First, we analyzed the expression of TLR7 in pDCs and CD4$^+$ DCs. As reported in previous studies (34, 35), we were able to detect the expression of TLR7 at both mRNA and protein levels (Supplemental Fig. 2). RNA interference cannot be used in primary pDCs because the RNA molecules induce type I IFN expression (39); therefore, we used a peptide that is fused to an antennapedia-derived cell permeant motif and inhibits MyD88 homodimerization by binding to the MyD88 TIR domain (40). pDCs from wild-type mice were cultured for 6 h in the presence of the MyD88 inhibitory peptide or the control peptide and activated with R837, a TLR7 ligand, for 24 h. The control peptide marginally affected IFN-β secretion induced by R837, and the MyD88 inhibitory peptide at 50 μM significantly reduced IFN-β production induced by R837 (Supplemental Fig. 3A). To evaluate the effects of the inhibitory peptide on cell viability, we counted the number of live cells using trypan blue staining (Supplemental Fig. 3B). Although stimulation with R837 partially induced cell death (41.3% ± 5.4%), cell viability was not changed by the addition of the inhibitory peptide at 50 μM (Supplemental Fig. 3B). MyD88 inhibitory peptide has no effects on polyinosinic/polycytidylic acid–induced IFN-β production in CD11c$^+$ DCs (Supplemental Fig. 3C). Next, we tested the effect of MyD88 inhibitory peptide on permissiveness and type I IFN production in MV-infected pDCs from CD150Tg/*Mavs*$^{-/-}$ mice. Although CD150Tg/*Mavs*$^{-/-}$ pDCs were not permissive to MV in the presence of control peptide, infection efficiency was increased 4-fold by treatment with MyD88 inhibitory peptide (Fig. 6A). As with pDCs, the infection efficiency of CD150Tg/*Mavs*$^{-/-}$ CD11c$^+$ DCs increased 3-fold by MyD88 inhibitory peptide treatment (Fig. 6B). When CD150Tg/*Mavs*$^{-/-}$ CD11c$^+$ DCs, CD4$^+$ DCs, and pDCs were pretreated with MyD88 inhibitory peptide, they did not induce type I IFN mRNA after MV infection (Fig. 6C–E). These data suggest that the MyD88 pathway is responsible for MV-induced type I IFN production in DCs under MAVS deficiency. To confirm that the MyD88 pathway is involved in type I IFN induction in MV-infected DCs, CD150Tg/*Myd88*$^{-/-}$ pDCs were infected with MV in vitro. *Ifn-β* mRNA expression was not induced in MV-infected CD150Tg/*Myd88*$^{-/-}$ pDCs (Fig. 6F).

Discussion

This study demonstrated that CD150Tg/*Mavs*$^{-/-}$ mice were not susceptible to MV infection in vivo (Fig. 1). This is an unexpected result because many reports have highlighted the important role of the RIG-I/MDA5-MAVS pathway in type I IFN production in MV-infected cells as a means to suppress MV replication. Ultimately, the MyD88 signal, rather than the MAVS signal, serves as a critical inducer of primary type I IFN for cell protection against

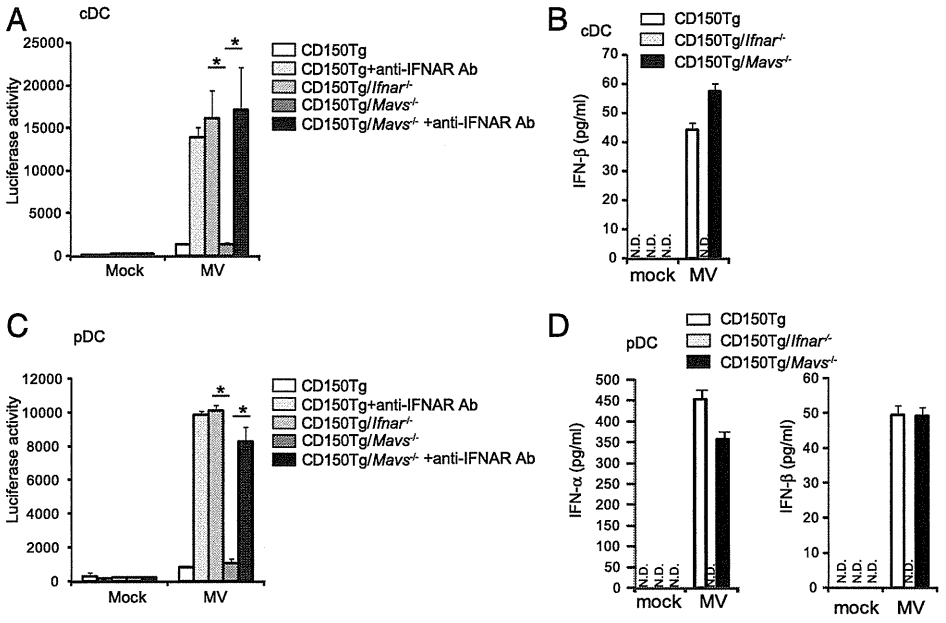

FIGURE 4. CD150Tg/*Mavs*$^{-/-}$ pDCs produced type I IFN in response to MV infection. The cDCs (**A**, **B**) or pDCs (**C**, **D**) isolated from CD150Tg, CD150Tg/*Ifnar*$^{-/-}$, or CD150Tg/*Mavs*$^{-/-}$ splenocytes were infected by MV (MOI of 0.25). At 24 h post infection, luciferase activity was measured (A, C). Production of type I IFN in culture supernatant was measured by ELISA (B, D). Data are means ± SD of three independent samples. N.D., Not detected.

MV replication in a mouse model. This finding would be a novel feature of MV, a negative single-stranded RNA virus, and has reminded us that cell-level studies on host innate immunity in coping with infection cannot always predict critical virus-sensing factors in whole-animal studies.

Because blockage of type I IFNR function resulted in permissiveness of CD150Tg/*Mavs*$^{-/-}$ mice to MV, MAVS-independent type I IFN induction protects neighboring cells (that express IFNAR) from MV infection (Fig. 2). Among the cell subsets tested, only pDCs and CD4$^+$ DCs from CD150Tg/*Mavs*$^{-/-}$ produced type I IFN after MV infection (Figs. 3–5). Treatment with inhibitory peptide for MyD88 drastically decreased type I IFN expression in CD150Tg/*Mavs*$^{-/-}$ DCs and rendered these cells MV permissive to MV (Fig. 6). These data indicate that the MyD88 pathway is involved in type I IFN induction in MV-infected pDCs and CD4$^+$ DCs under a MAVS-deficient state. The results were confirmed with CD150/*Myd88*$^{-/-}$ mice (Fig. 6F). In this context, the MyD88 pathway plays a primary role in the initial phase of MV protection in vivo. However, CD150Tg/*Myd88*$^{-/-}$ mice were not permissive to MV in vivo (data not shown), suggesting that not only MyD88 in pDCs/CD4$^+$ DCs but also MAVS in other cells contributes to the protection against systemic infection by MV. Because the MyD88 pathway participates in the initial type I IFN induction in pDCs, only a very weak but significant luciferase activity was detected in the spleen of CD150Tg/*Mavs*$^{-/-}$ mice at day 1 after inoculation (Fig. 1C). Moreover, CD8α$^+$ DCs and DN DCs from CD150Tg/*Mavs*$^{-/-}$ mice could not induce *Ifn-β* mRNA expression in response to MV infection in vitro (Fig. 5). These results suggest that the MAVS pathway also participates in host defense against MV infection as an alternative pathway in splenic DCs, at least in these experimental conditions.

Another target cell of MV infection in nonhuman primates is the AM (18). AMs in the CD150Tg/*Ifnar*$^{-/-}$ mouse model are also permissive to MV infection (17). AMs derived from CD150Tg/*Mavs*$^{-/-}$ mice were permissive to MV infection in vitro (data not shown). This result is consistent with a previous report indicating that the RLR-MAVS pathway is predominantly used for type I IFN induction in virus-infected AMs (41). However, intratracheal inoculation with MV in CD150Tg/*Mavs*$^{-/-}$ mice resulted in a lower luciferase activity in AMs from CD150Tg/*Mavs*$^{-/-}$ mice than in those from CD150Tg/*Ifnar*$^{-/-}$ mice (data not shown), similar to the results from i.p. inoculation. These data indicate that a cell population other than AMs produces type I IFN in MV-infected lungs. In this case, pDCs in lung might act as IFN-producing cells, because pDCs in lung are reported to produce type I IFN and act as immune system defenders against infection (41). Taken together, the recognition pathways for MV to induce type I IFN differ among cell types. Existence of the several alternative pathways might engage the protection from systemic MV infection (Supplemental Fig. 4).

In CD8α$^-$ DCs and pDCs, the TLR-MyD88 pathway is preferentially used to induce type I IFN in response to infections. TLR7, a sensor for viral RNA, is known to be expressed specifically in these DC subsets (34, 35) (Supplemental Fig. 2). The restricted expression pattern of TLR7 seems to reflect the ability of CD4$^+$ DCs and pDCs to produce type I IFN in MV-infected CD150Tg/*Mavs*$^{-/-}$. Therefore, TLR7 may be one of the candidate receptors for recognition of MV RNA. Because viral RNA is recognized mainly through the RLR-MAVS pathway in CD4$^+$ DCs at steady state (35), it would be difficult to examine the role of the TLR7-MyD88 pathway in CD4$^+$ DCs during viral infection in WT mice. Thus, our assay system using CD150Tg mice crossed with given knockout mice is a powerful tool to investigate the signaling pathway for host defense against MV infection.

Previous studies were mainly done using bone marrow–derived DCs (BMDCs) to analyze the immunosuppressive effects of MV in a mouse model (16, 42, 43). However, BMDCs from CD150Tg/*Mavs*$^{-/-}$ mice completely lacked the ability to produce type I IFN in response to MV infection. In contrast to the results in splenic DCs (44). Because the expression profile of pattern-recognition receptors in BMDCs was different from the profile in splenic DCs (34, 35, 45), it is reasonable to think that each cell type has its own unique type I IFN induction pathway in response to viral infection. Therefore, further investigations on immunosuppression and immunopromotion of MV in infected DCs should be performed using splenic DCs, taking into consideration the properties of resident DCs.

In this study, we used recombinant MV-luciferase that expresses the reporter *Renilla* luciferase from the first gene position of MV genome (29). The MV-luciferase is suitable to evaluate the efficiency of infection in vivo and in vitro correctly because the assay

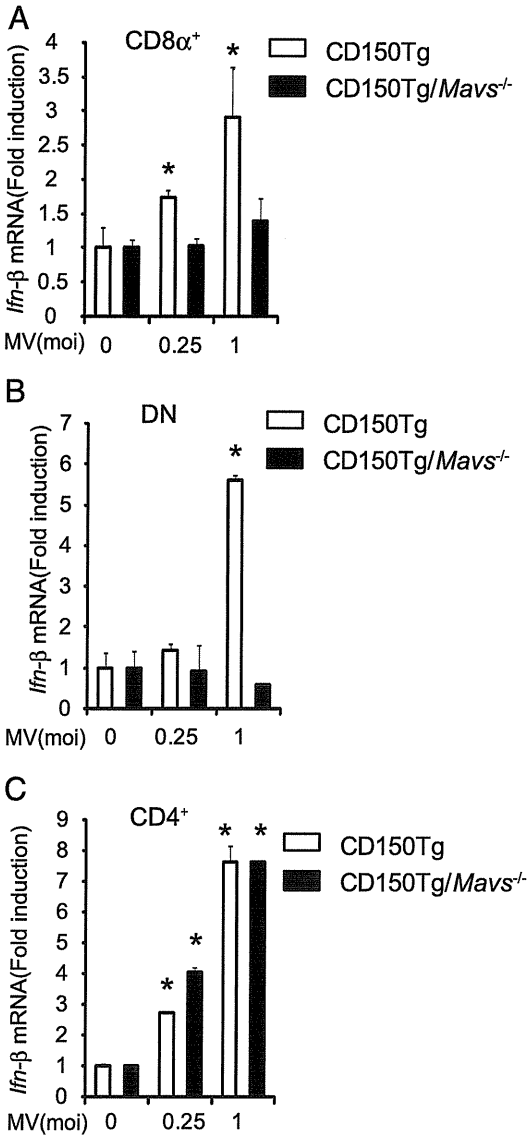

FIGURE 5. MV-infected CD150Tg/*Mavs*$^{-/-}$ CD4$^+$ DCs expressed type I IFN mRNA. CD8α$^+$ DCs (**A**), DN DCs (**B**), and CD4$^+$ DCs (**C**) were isolated by MACS beads. Cells were infected with MV (MOI of 0.25 or 1.0) for 9 h, and levels of *Ifn-β* mRNA were measured by real-time PCR. Data are means ± SD of three independent samples. *A *t* test between 0 h. p.i. and the indicate time in respective mouse line is $p < 0.05$.

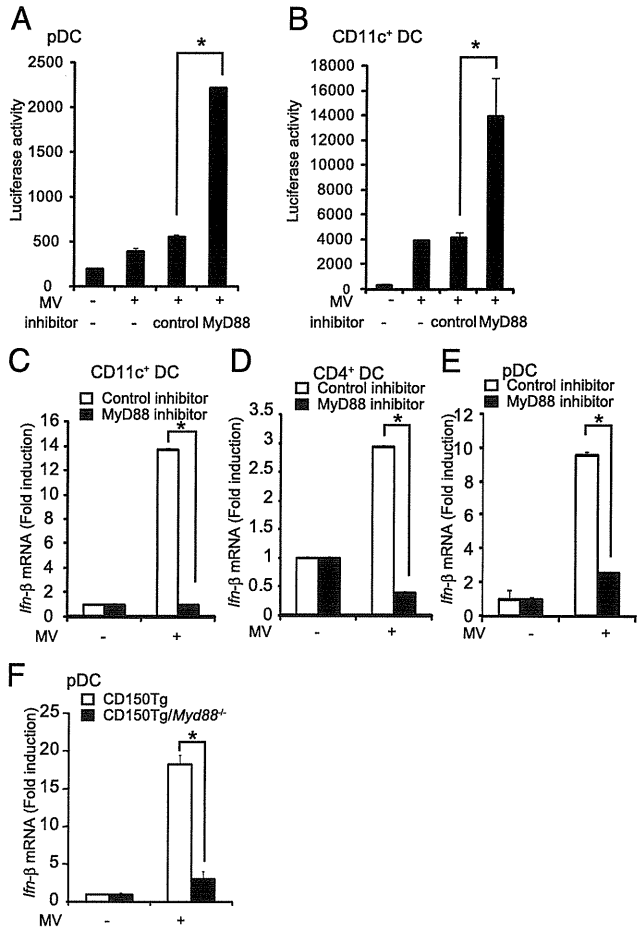

FIGURE 6. The MyD88 pathway is responsible for MV-induced type I IFN induction in CD150Tg/*Mavs*$^{-/-}$ DCs. (**A**) pDCs were isolated by FACS or (**B**) CD11c$^+$ DCs were isolated by MACS beads from CD150Tg/*Mavs*$^{-/-}$ splenocytes. Cells were treated with 50 μM of the control peptide or 50 μM of the MyD88 inhibitory peptide for 6 h and then infected with MV (MOI of 0.25). After 18 h, luciferase activity was measured. Data are means ± SD of three independent samples. CD150Tg/*Mavs*$^{-/-}$ CD11c$^+$ DCs (**C**), CD4$^+$ DCs (**D**), and pDCs (**E**) were pretreated with 50 μM control peptide or 50 μM MyD88 inhibitory peptide for 6 h following infection with MV (MOI of 0.25) for 9 h. Expression levels of *Ifn-β* mRNA were measured by real-time PCR. Expression levels of data are means ± SD of three independent samples. (**F**) *Ifn-β* mRNA expression in MV-infected CD150Tg and CD150Tg/*Myd88*$^{-/-}$ pDCs. pDCs were infected with MV (MOI = 0.25) for 9 h. Expression levels of *Ifn-β* mRNA were measured by real-time PCR. Expression levels of data are means ± SD of three independent samples. *$p < 0.05$.

system worked well using the CD150Tg/*Ifnar*$^{-/-}$ mouse model. Luciferase activity and MV-P mRNA in CD150Tg/*Ifnar*$^{-/-}$ was significantly increased compared with CD150Tg mice during infection (Fig. 1A, 1B and data not shown). Luciferase activity obtained from MV-infected Vero/CD150 cells was correlated with viral titer in culture supernatant from MV-infected cells (data not shown). Recombinant MV strains expressing a foreign gene from a first gene position of the MV genome were used in several groups for in vivo infection assay without any problem (17, 18, 24). However, the infection efficiency of recombinant *Morbillivirus* expressing a foreign gene from position one is reported to be attenuated in vivo (46), which is well reflected in the relatively low virus titer observed in the spleen from CD150Tg mice infected with MV-luciferase.

In mouse models, the route of MV inoculation does not always reflect the natural infection route in human MV infection. Our results obtained from experiments using the i.p. infection model also may not faithfully reflect the process of natural MV infection involving epithelial cells in humans. However, as described above, intratracheal and i.p. administration gave rise to similar results in MV infection. This issue may reflect the viral strategy of targeting myeloid cells for initial propagation. Injected MV reaches DCs or macrophages without affecting other bystander cells in any route of MV administration. However, this is not the case in other virus species with different target cells for initial infection.

We conclude that MyD88-dependent type I IFN production in CD4$^+$ DCs and pDCs results in initial protection against MV; thereafter, the produced type I IFN induces an antiviral state in the neighboring cells, expressing IFNAR in the mouse model.

Acknowledgments

We thank Drs. T. Taniguchi (University of Tokyo, Tokyo, Japan) and S. Akira (Osaka University, Osaka, Japan) for providing *Irf3*$^{-/-}$/*Irf7*$^{-/-}$ and *Myd88*$^{-/-}$ mice, respectively, for this study, and Dr. Y. Yanagi (Kyushu University, Fukuoka, Japan) for providing MV-luciferase.

Disclosures

The authors have no financial conflicts of interest.

References

1. Honda, K., A. Takaoka, and T. Taniguchi. 2006. Type I interferon [corrected] gene induction by the interferon regulatory factor family of transcription factors. *Immunity* 25: 349–360.
2. Yoneyama, M., K. Onomoto, and T. Fujita. 2008. Cytoplasmic recognition of RNA. *Adv. Drug Deliv. Rev.* 60: 841–846.
3. Takeuchi, O., and S. Akira. 2009. Innate immunity to virus infection. *Immunol. Rev.* 227: 75–86.
4. Yamamoto, M., S. Sato, K. Mori, K. Hoshino, O. Takeuchi, K. Takeda, and S. Akira. 2002. Cutting edge: a novel Toll/IL-1 receptor domain-containing adapter that preferentially activates the IFN-beta promoter in the Toll-like receptor signaling. *J. Immunol.* 169: 6668–6672.
5. Oshiumi, H., M. Matsumoto, K. Funami, T. Akazawa, and T. Seya. 2003. TICAM-1, an adaptor molecule that participates in Toll-like receptor 3-mediated interferon-beta induction. *Nat. Immunol.* 4: 161–167.
6. Kawai, T., K. Takahashi, S. Sato, C. Coban, H. Kumar, H. Kato, K. J. Ishii, O. Takeuchi, and S. Akira. 2005. IPS-1, an adaptor triggering RIG-I- and Mda5-mediated type I interferon induction. *Nat. Immunol.* 6: 981–988.
7. Yamamoto, M., S. Sato, H. Hemmi, K. Hoshino, T. Kaisho, H. Sanjo, O. Takeuchi, M. Sugiyama, M. Okabe, K. Takeda, and S. Akira. 2003. Role of adaptor TRIF in the MyD88-independent toll-like receptor signaling pathway. *Science* 301: 640–643.
8. Kumar, H., T. Kawai, H. Kato, S. Sato, K. Takahashi, C. Coban, M. Yamamoto, S. Uematsu, K. J. Ishii, O. Takeuchi, and S. Akira. 2006. Essential role of IPS-1 in innate immune responses against RNA viruses. *J. Exp. Med.* 203: 1795–1803.
9. Ikegame, S., M. Takeda, S. Ohno, Y. Nakatsu, Y. Nakanishi, and Y. Yanagi. 2010. Both RIG-I and MDA5 RNA helicases contribute to the induction of alpha/beta interferon in measles virus-infected human cells. *J. Virol.* 84: 372–379.
10. Berghäll, H., J. Sirén, D. Sarkar, I. Julkunen, P. B. Fisher, R. Vainionpää, and S. Matikainen. 2006. The interferon-inducible RNA helicase, mda-5, is involved in measles virus-induced expression of antiviral cytokines. *Microbes Infect.* 8: 2138–2144.
11. Griffin, D. E. 1995. Immune responses during measles virus infection. *Curr. Top. Microbiol. Immunol.* 191: 117–134.
12. Tatsuo, H., N. Ono, K. Tanaka, and Y. Yanagi. 2000. SLAM (CDw150) is a cellular receptor for measles virus. *Nature* 406: 893–897.
13. Mühlebach, M. D., M. Mateo, P. L. Sinn, S. Prüfer, K. M. Uhlig, V. H. Leonard, C. K. Navaratnarajah, M. Frenzke, X. X. Wong, B. Sawatsky, et al. 2011. Adherens junction protein nectin-4 is the epithelial receptor for measles virus. *Nature* 480: 530–533.
14. Noyce, R. S., D. G. Bondre, M. N. Ha, L. T. Lin, G. Sisson, M. S. Tsao, and C. D. Richardson. 2011. Tumor cell marker PVRL4 (nectin 4) is an epithelial cell receptor for measles virus. *PLoS Pathog.* 7: e1002240.
15. Delpeut, S., R. S. Noyce, R. W. Siu, and C. D. Richardson. 2012. Host factors and measles virus replication. *Curr Opin Virol* 2: 773–783.
16. Shingai, M., N. Inoue, T. Okuno, M. Okabe, T. Akazawa, Y. Miyamoto, M. Ayata, K. Honda, M. Kurita-Taniguchi, M. Matsumoto, et al. 2005. Wild-type measles virus infection in human CD46/CD150-transgenic mice: CD11c-positive dendritic cells establish systemic viral infection. *J. Immunol.* 175: 3252–3261.
17. Ferreira, C. S., M. Frenzke, V. H. Leonard, G. G. Welstead, C. D. Richardson, and R. Cattaneo. 2010. Measles virus infection of alveolar macrophages and dendritic cells precedes spread to lymphatic organs in transgenic mice expressing human signaling lymphocytic activation molecule (SLAM, CD150). *J. Virol.* 84: 3033–3042.
18. Lemon, K., R. D. de Vries, A. W. Mesman, S. McQuaid, G. van Amerongen, S. Yüksel, M. Ludlow, L. J. Rennick, T. Kuiken, B. K. Rima, et al. 2011. Early target cells of measles virus after aerosol infection of non-human primates. *PLoS Pathog.* 7: e1001263.
19. Mesman, A. W., R. D. de Vries, S. McQuaid, W. P. Duprex, R. L. de Swart, and T. B. Geijtenbeek. 2012. A prominent role for DC-SIGN+ dendritic cells in initiation and dissemination of measles virus infection in non-human primates. *PLoS ONE* 7: e49573.
20. Schneider-Schaulies, S., I. M. Klagge, and V. ter Meulen. 2003. Dendritic cells and measles virus infection. *Curr. Top. Microbiol. Immunol.* 276: 77–101.
21. Servet-Delprat, C., P. O. Vidalain, H. Valentin, and C. Rabourdin-Combe. 2003. Measles virus and dendritic cell functions: how specific response cohabits with immunosuppression. *Curr. Top. Microbiol. Immunol.* 276: 103–123.
22. Welstead, G. G., C. Iorio, R. Draker, J. Bayani, J. Squire, S. Vongpunsawad, R. Cattaneo, and C. D. Richardson. 2005. Measles virus replication in lymphatic cells and organs of CD150 (SLAM) transgenic mice. *Proc. Natl. Acad. Sci. USA* 102: 16415–16420.
23. Sellin, C. I., N. Davoust, V. Guillaume, D. Baas, M. F. Belin, R. Buckland, T. F. Wild, and B. Horvat. 2006. High pathogenicity of wild-type measles virus infection in CD150 (SLAM) transgenic mice. *J. Virol.* 80: 6420–6429.
24. Ohno, S., N. Ono, F. Seki, M. Takeda, S. Kura, T. Tsuzuki, and Y. Yanagi. 2007. Measles virus infection of SLAM (CD150) knockin mice reproduces tropism and immunosuppression in human infection. *J. Virol.* 81: 1650–1659.
25. Akazawa, T., T. Ebihara, M. Okuno, Y. Okuda, M. Shingai, K. Tsujimura, T. Takahashi, M. Ikawa, M. Okabe, N. Inoue, et al. 2007. Antitumor NK activation induced by the Toll-like receptor 3-TICAM-1 (TRIF) pathway in myeloid dendritic cells. *Proc. Natl. Acad. Sci. USA* 104: 252–257.
26. Oshiumi, H., M. Okamoto, K. Fujii, T. Kawanishi, M. Matsumoto, S. Koike, and T. Seya. 2011. The TLR3/TICAM-1 pathway is mandatory for innate immune responses to poliovirus infection. *J. Immunol.* 187: 5320–5327.
27. Kobune, F., H. Sakata, and A. Sugiura. 1990. Marmoset lymphoblastoid cells as a sensitive host for isolation of measles virus. *J. Virol.* 64: 700–705.
28. Takeda, M., K. Takeuchi, N. Miyajima, F. Kobune, Y. Ami, N. Nagata, Y. Suzaki, Y. Nagai, and M. Tashiro. 2000. Recovery of pathogenic measles virus from cloned cDNA. *J. Virol.* 74: 6643–6647.
29. Takeda, M., M. Tahara, T. Hashiguchi, T. A. Sato, F. Jinnouchi, S. Ueki, S. Ohno, and Y. Yanagi. 2007. A human lung carcinoma cell line supports efficient measles virus growth and syncytium formation via a SLAM- and CD46-independent mechanism. *J. Virol.* 81: 12091–12096.
30. Shingai, M., T. Ebihara, N. A. Begum, A. Kato, T. Honma, K. Matsumoto, H. Saito, H. Ogura, M. Matsumoto, and T. Seya. 2007. Differential type I IFN-inducing abilities of wild-type versus vaccine strains of measles virus. *J. Immunol.* 179: 6123–6133.
31. Sheehan, K. C., K. S. Lai, G. P. Dunn, A. T. Bruce, M. S. Diamond, J. D. Heutel, C. Dungo-Arthur, J. A. Carrero, J. M. White, P. J. Hertzog, and R. D. Schreiber. 2006. Blocking monoclonal antibodies specific for mouse IFN-alpha/beta receptor subunit 1 (IFNAR-1) from mice immunized by in vivo hydrodynamic transfection. *J. Interferon Cytokine Res.* 26: 804–819.
32. Vremec, D., J. Pooley, H. Hochrein, L. Wu, and K. Shortman. 2000. CD4 and CD8 expression by dendritic cell subtypes in mouse thymus and spleen. *J. Immunol.* 164: 2978–2986.
33. Asselin-Paturel, C., A. Boonstra, M. Dalod, I. Durand, N. Yessaad, C. Dezutter-Dambuyant, A. Vicari, A. O'Garra, C. Biron, F. Brière, and G. Trinchieri. 2001. Mouse type I IFN-producing cells are immature APCs with plasmacytoid morphology. *Nat. Immunol.* 2: 1144–1150.
34. Edwards, A. D., S. S. Diebold, E. M. Slack, H. Tomizawa, H. Hemmi, T. Kaisho, S. Akira, and C. Reis e Sousa. 2003. Toll-like receptor expression in murine DC subsets: lack of TLR7 expression by CD8 alpha+ DC correlates with unresponsiveness to imidazoquinolines. *Eur. J. Immunol.* 33: 827–833.
35. Luber, C. A., J. Cox, H. Lauterbach, B. Fancke, M. Selbach, J. Tschopp, S. Akira, M. Wiegand, H. Hochrein, M. O'Keeffe, and M. Mann. 2010. Quantitative proteomics reveals subset-specific viral recognition in dendritic cells. *Immunity* 32: 279–289.
36. Hemmi, H., T. Kaisho, O. Takeuchi, S. Sato, H. Sanjo, K. Hoshino, T. Horiuchi, H. Tomizawa, K. Takeda, and S. Akira. 2002. Small anti-viral compounds activate immune cells via the TLR7 MyD88-dependent signaling pathway. *Nat. Immunol.* 3: 196–200.
37. Heil, F., H. Hemmi, H. Hochrein, F. Ampenberger, C. Kirschning, S. Akira, G. Lipford, H. Wagner, and S. Bauer. 2004. Species-specific recognition of single-stranded RNA via toll-like receptor 7 and 8. *Science* 303: 1526–1529.
38. Diebold, S. S., T. Kaisho, H. Hemmi, S. Akira, and C. Reis e Sousa. 2004. Innate antiviral responses by means of TLR7-mediated recognition of single-stranded RNA. *Science* 303: 1529–1531.
39. Hornung, V., M. Guenthner-Biller, C. Bourquin, A. Ablasser, M. Schlee, S. Uematsu, A. Noronha, M. Manoharan, S. Akira, A. de Fougerolles, et al. 2005. Sequence-specific potent induction of IFN-alpha by short interfering RNA in plasmacytoid dendritic cells through TLR7. *Nat. Med.* 11: 263–270.
40. Loiarro, M., C. Sette, G. Gallo, A. Ciacci, N. Fantò, D. Mastroianni, P. Carminati, and V. Ruggiero. 2005. Peptide-mediated interference of TIR domain dimerization in MyD88 inhibits interleukin-1-dependent activation of NF-kappaB. *J. Biol. Chem.* 280: 15809–15814.
41. Kumagai, Y., O. Takeuchi, H. Kato, H. Kumar, K. Matsui, E. Morii, K. Aozasa, T. Kawai, and S. Akira. 2007. Alveolar macrophages are the primary interferon-alpha producer in pulmonary infection with RNA viruses. *Immunity* 27: 240–252.
42. Hahm, B., N. Arbour, and M. B. Oldstone. 2004. Measles virus interacts with human SLAM receptor on dendritic cells to cause immunosuppression. *Virology* 323: 292–302.
43. Koga, R., S. Ohno, S. Ikegame, and Y. Yanagi. 2010. Measles virus-induced immunosuppression in SLAM knock-in mice. *J. Virol.* 84: 5360–5367.
44. Takaki, H., K. Honda, K. Atarashi, F. Kobayashi, T. Ebihara, H. Oshiumi, M. Matsumoto, M. Shingai, and T. Seya. 2013. MAVS-dependent IRF3/IRF7 bypass of interferon β-induction restricts the response to measles infection in CD150Tg mouse bone marrow-derived dendritic cells. *Molec. Immunol.* In press.
45. Datta, S. K., V. Redecke, K. R. Prilliman, K. Takabayashi, M. Corr, T. Tallant, J. DiDonato, R. Dziarski, S. Akira, S. P. Schoenberger, and E. Raz. 2003. A subset of Toll-like receptor ligands induces cross-presentation by bone marrow-derived dendritic cells. *J. Immunol.* 170: 4102–4110.
46. von Messling, V., D. Milosevic, and R. Cattaneo. 2004. Tropism illuminated: lymphocyte-based pathways blazed by lethal morbillivirus through the host immune system. *Proc. Natl. Acad. Sci. USA* 101: 14216–14221.

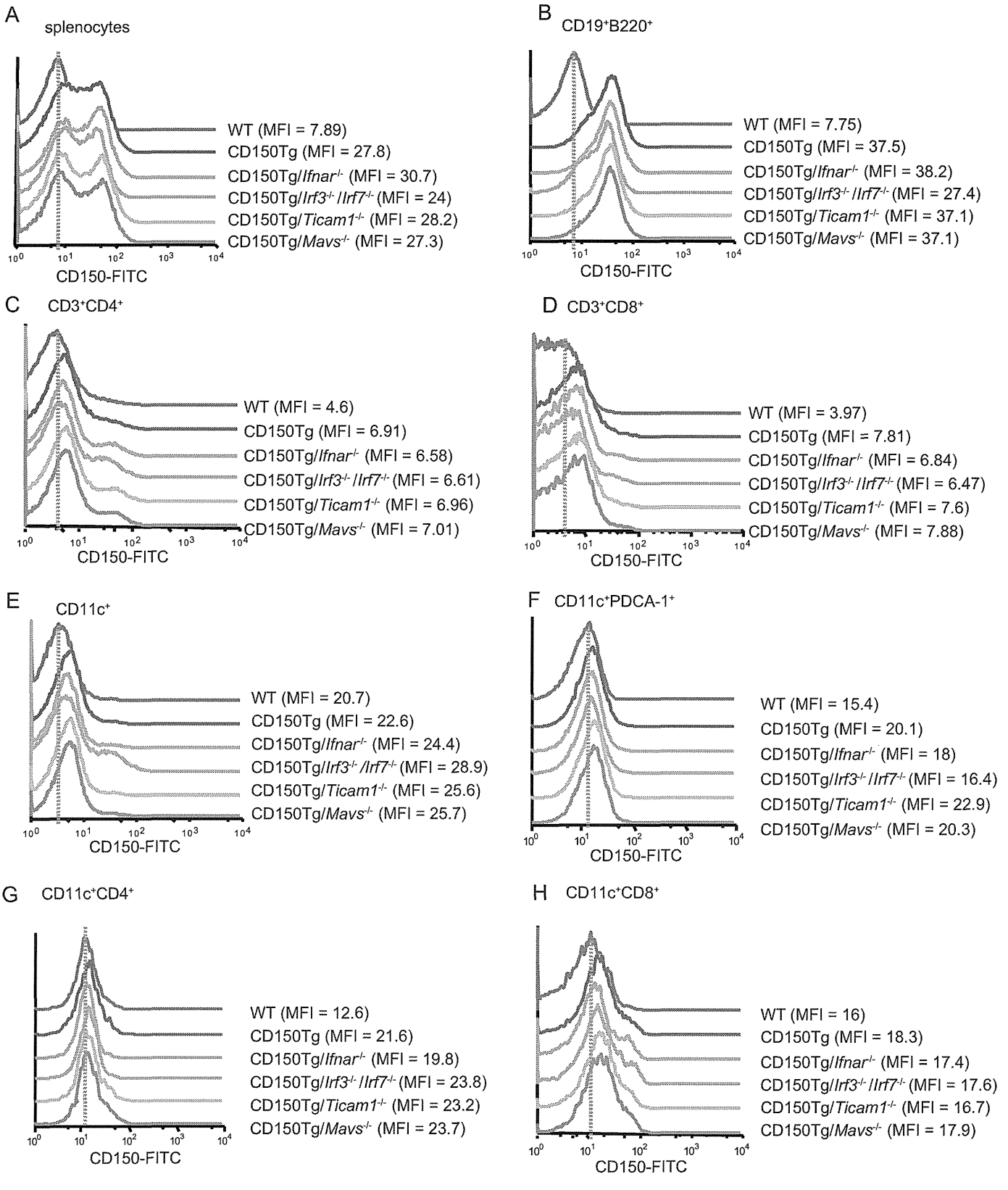

Supplemental Figure 1. Human CD150 expression in splenocytes.

Expression levels of human CD150 in variouse splenocytes derived from wild-type, CD150Tg, CD150Tg/*Ifnar*$^{-/-}$, CD150Tg/*Irf3*$^{-/-}$/*Irf7*$^{-/-}$, CD150Tg/*Mavs*$^{-/-}$ and CD150Tg/*Ticam1*$^{-/-}$ mice were measured by FACS. (A) Whole splenocytes, (B) CD19^{+}B220^{+} B cells, (C) CD3^{+}CD4^{+} T cells, (D) CD3^{+}CD8^{+} T cells, (E) CD11c^{+} DCs, (F) CD11c^{+}PDCA-1^{+} pDCs, (G) CD11c^{+}CD4^{+} DCs, (H) CD11c^{+}CD8α^{+} DCs and (I) CD11c^{+} CD4^{-}CD8α^{-} DN DCs. Mean fluorescence intensities of CD150-FITC from each population are in the histograms. One representative expriment of two is shown.

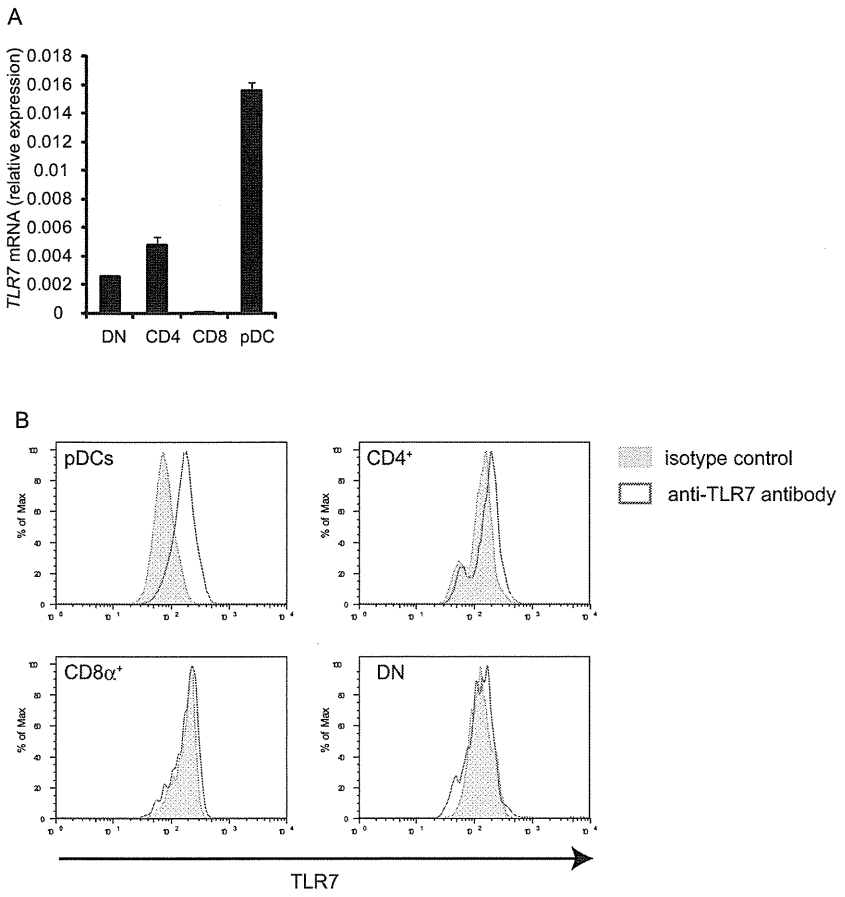

Supplemental Figure 2. TLR7 expression in DC subsets.

(A) DC subsets were isolated from splecnoytes of wild-type mice by MACS beads or FACS sorting and levels of *Tlr7* mRNA in each subset were quantified by real-time PCR. *Tlr7* mRNA expression in shown as relative expression to β-*actin*. Data are means ± SD of three independent samples.(B) DCs were stained with anti-TLR7 antibody (red line) or isotype control (gray line). Expression of TLR7 protein in each subset was analyzed by FACS. One representative experiment of two is shown.

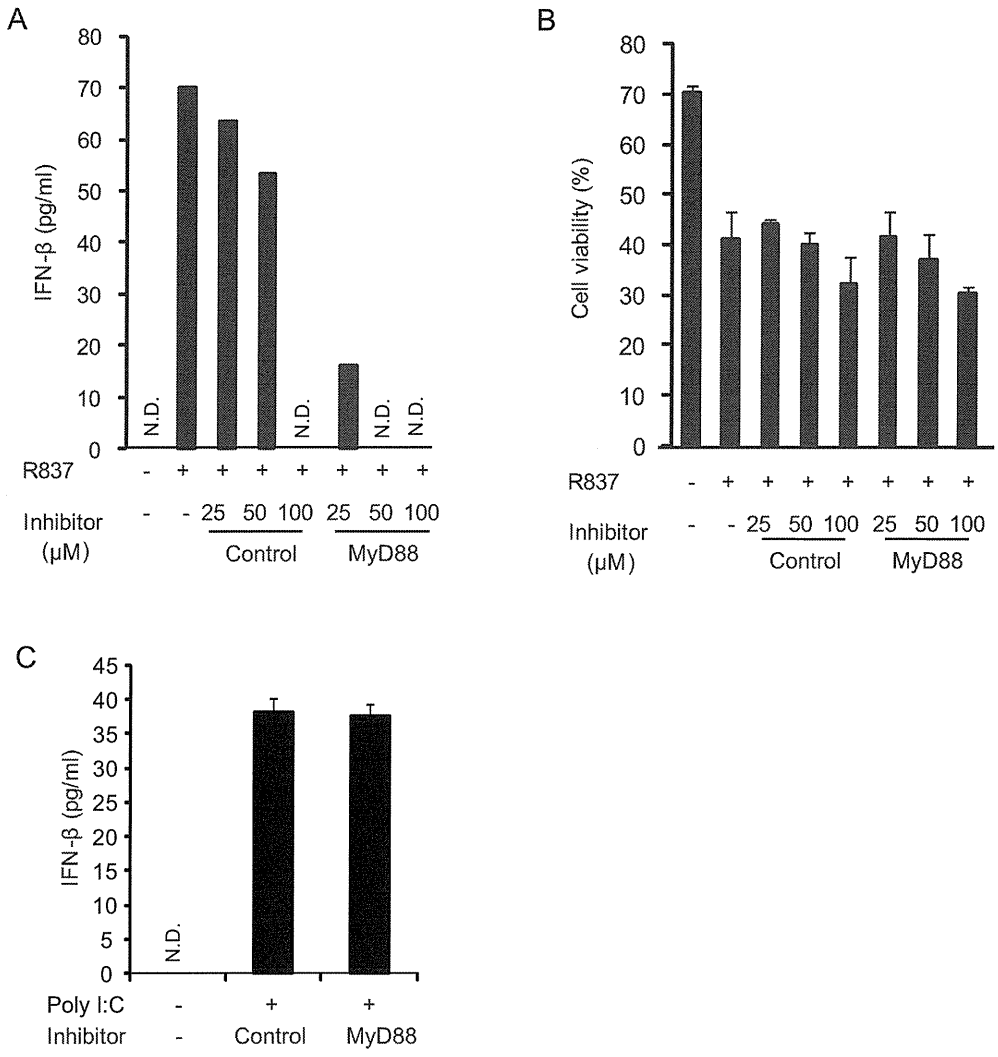

Supplemental Figure 3. Effect of MyD88 inhibitory peptide on IFN-β prodution.

Aria-sorted WT pDCs were pretreated with the indicated concentration of control peptide or MyD88 inhibitory peptide for 6 hours following stimulated with 2 μg/ml of R837 for 24 hours. (A) IFN-β in the culture supernatants were measured by ELISA. (B) Cells were stained with trypan blue and live cells were counted. Data are shown as the percentage of cells viability and means ± SD of three independent samples. (C) $CD11c^+$ DCs were pretreated with 50 μM of control or MyD88 inhibitory peptide for 6 hours following stimulated with 50 μg/ml of poly I:C for 24 hours. IFN-β in the culture supernatants were measured by ELISA.

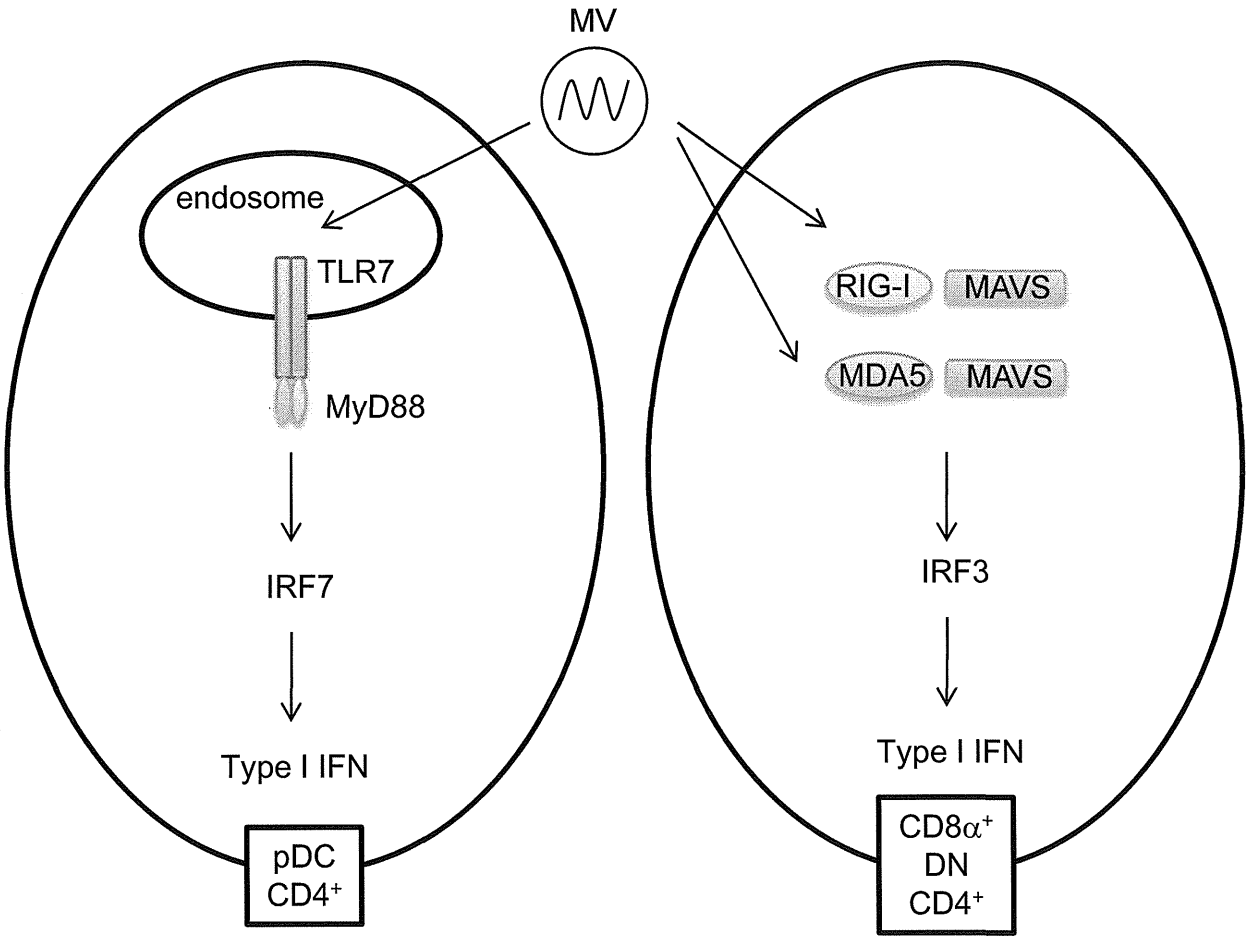

Supplemental Figure 4. MV recognition in murine dendritic cells.
MV RNA is recognized by cytosolic RNA sensors, RIG-I and MDA5, in human epithelia cells. In murine $CD4^+$, $CD8\alpha^+$ and DN DCs, the RLR-MAVS pathway is involved in MV-induced type I IFN induction. In $CD4^+$ DCs and pDCs, the TLR7-MyD88 pathway also participates in the type I IFN induction. The recognition pathways of MV RNA are different from each cell type and several pathways of type I IFN induction engage protection against MV infection in this mouse model.

JVI Journals.ASM.org

Herpesvirus 6 Glycoproteins B (gB), gH, gL, and gQ Are Necessary and Sufficient for Cell-to-Cell Fusion

Yuki Tanaka,[a] Tadahiro Suenaga,[a,b] Misako Matsumoto,[c] Tsukasa Seya,[c] Hisashi Arase[a,b,d]

Department of Immunochemistry, Research Institute for Microbial Diseases, Osaka University, Osaka, Japan[a]; Laboratory of Immunochemistry, WPI Immunology Frontier Research Center, Osaka University, Osaka, Japan[b]; Department of Microbiology and Immunology, Graduate School of Medicine, Hokkaido University, Sapporo, Japan[c]; CREST, JST, Tokyo, Japan[d]

The human herpesvirus 6 (HHV-6) envelope glycoprotein gH/gL/gQ1/gQ2 complex associates with host cell CD46 as its cellular receptor. Although gB has been suggested to be involved in HHV-6 infection, its function in membrane fusion has remained unclear. Here, we have developed an HHV-6A (strain GS)and HHV-6B (strain Z29) virus-free cell-to-cell fusion assay and demonstrate that gB and the gH/gL/gQ1/gQ2 complex are the minimum components required for membrane fusion by HHV-6.

Human herpesvirus 6 (HHV-6), betaherpesvirus subfamily (1), includes two species, A (HHV-6A) and B (HHV-6B) (2–4). HHV-6B mainly infects immune cells, such as $CD4^+$ T-lymphocytes, monocytes, and dendritic cells, and also causes exanthema subitum during primary infection in children (5). HHV-6B can reactivate from latency in immunocompromised patients and cause pneumonitis, hepatitis, and encephalitis (6, 7). However, the molecular basis of HHV-6A pathogenicity is unclear.

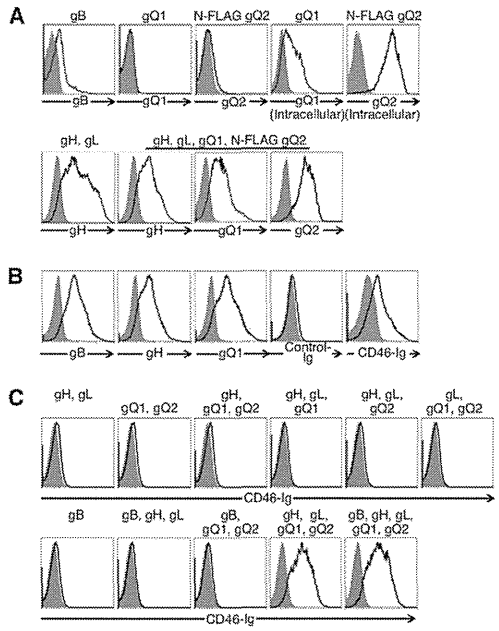

FIG 1 Flow cytometric analyses of cell surface expression of viral glycoproteins in cells transfected with plasmids expressing the glycoproteins. The transfected glycoprotein(s) is shown at the top of each figure panel. gQ2 was FLAG tagged. (A) Expression of HHV-6B glycoprotein(s) in 293T cells transfected with plasmids expressing HHV-6B glycoprotein(s) (black lines) or mock transfected (gray-shaded areas). Cells were stained with anti-gB (H-AR-2; Bioworld Consulting Laboratories), anti-gH, anti-gQ1 (2D6; NIH, AIDS Reagent Program), or FLAG (L5; Biolegend) MAb followed by staining with anti-mouse IgG antibody. (B) Cell surface expresson of HHV-6B glycoproteins in virus-infected cells and association of CD46 with HHV-6B-infected cells. HHV-6B-infected (black lines) or mock-infected (gray-shaded areas) Molt-3 cells were stained with anti-gB, anti-gH, or anti-gQ1 MAb followed by staining with anti-mouse IgG antibody and either CD46-Ig or control Ig (VZV gB-Ig) followed by staining with anti-human IgG Fc portion antibody. (C) Association of CD46 with HHV-6B glycoproteins. 293T cells that were transfected with plasmids expressing HHV-6B glycoprotein(s) (black lines) or mock transfected (gray-shaded areas) were stained with CD46-Ig.

The association of several viral glycoproteins with their respective cellular receptors induces virus envelope-cell membrane fusion during viral entry. It has been reported that HHV-6 gH/gL forms a complex with gQ1 and gQ2 and that this complex binds to CD46, which has been reported to function as a cellular receptor for HHV-6 (8–11). gB and a gH/gL complex are conserved in all herpesviruses and thought to play a pivotal role in membrane fusion and herpesvirus infection (12–17). Studies of gBs and gHs of other herpesviruses have elucidated the molecular mechanisms of virus envelope-cell membrane fusion (18–21). Although some antibodies against HHV-6 gB have been reported to block HHV-6B infection (22, 23), the function of HHV-6 gB during viral infection remains unclear.

To identify the requirement of HHV-6 glycoproteins for virus-induced membrane fusion during the virus infection, each of the glycoproteins was amplified and expressed from HHV-6B (Z29). Briefly, the genomic sequences of gH, gL, gO, gQ1, and gQ2 were amplified from total DNA of HHV-6B-infected Molt3 cells (Riken BRC, Tsukuba, Japan) and cloned into pCAGGS-MCS expression vector (24). For detection purposes, the FLAG epitope was inserted in frame at the N termini of gO and gQ2 genes. The full-length gB gene containing a promoter and poly(A) tail sequences was amplified by recombinant PCR using plasmids containing partial gB sequences (nucleotides [nt] +1 to +1718 and +1713 to +2493). The purified PCR product was used for transient transfection of 293T cells. Expression of transfected genes was analyzed by flow cytometry. gB and the gH/gL complex were detected on the cell surface using anti-gB monoclonal antibody (MAb) and gHA2 antibody, respectively (Fig. 1A) (25). Cells transfected with plasmid encoding gQ1 or N-terminal FLAG-tagged gQ2 ex-

Received 4 June 2013 Accepted 16 July 2013
Published ahead of print 24 July 2013
Address correspondence to Tadahiro Suenaga, tsue@biken.osaka-u.ac.jp.

doi:10.1128/JVI.01427-13

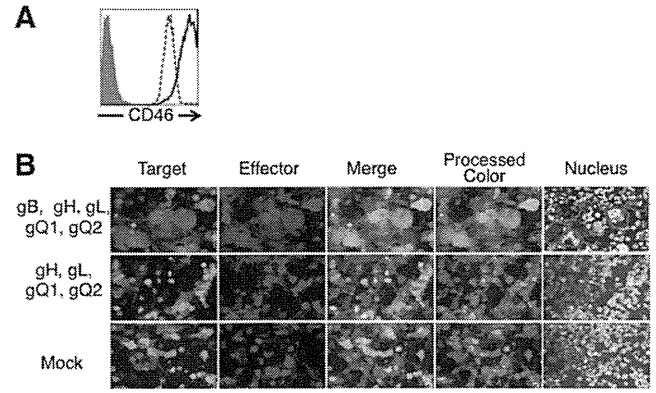

FIG 2 Fluorescence microscopy of fusion of 293T effector and target cells. (A) To quantify CD46 expression on the surface of 293T cells, 293T cells were stained with anti-CD46 MAb (J4.48; Coulter) (dotted line) or with isotype control antibody (gray-shaded area), and CD46-transfected 293T cells were stained with anti-CD46 MAb (solid line) and analyzed by flow cytometry. (B) 293T effector cells were transfected with plasmids expressing HHV-6B glycoproteins or mock transfected with a plasmid expressing DsRed. 293T target cells were transfected with a plasmid expressing CD46 and a plasmid expressing GFP. After 72 h coculture, cells were analyzed by fluorescence microscopy. Cell nuclei were stained with Hoechst 33258 fluorescence dye; blue fluorescence from nuclei appears gray. Fused cells are delineated by red lines.

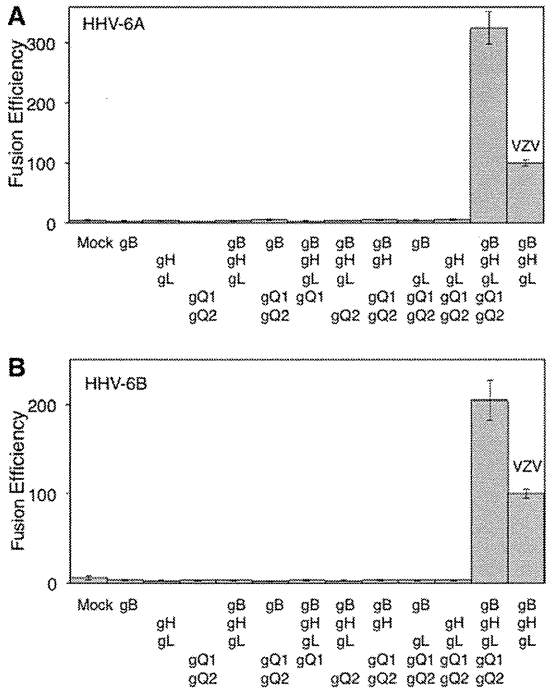

FIG 3 Quantification of cell-to-cell fusion mediated by HHV-6 glycoproteins. (A) 293T effector cells transfected with plasmids expressing HHV-6A glycoproteins, T7 polymerase, and *Renilla* luciferase were cocultured with 293T target cells transfected with plasmids expressing CD46 and firefly luciferase. After 72 h coculture, both luciferase signals were measured. The relative fusion efficiency was calculated as follows: [(HHV-6 firefly luciferase activity/HHV-6 *Renilla* luciferase activity) × 100]/(VZV firefly luciferase activity/VZV *Renilla* luciferase activity). (B) Quantification of cell-to-cell fusion efficiency mediated by HHV-6B glycoproteins was performed as described for HHV-6A in the panel A legend. Error bars show the means ± standard deviations (SD) of the results determined with quadruplicated samples. Data are representative of at least three independent experiments.

pressed the corresponding proteins. gQ1 and gQ2 were detected intracellularly but not on the cell surface, although they were detected on the surface of cells cotransfected with gH and gL. N-terminal FLAG-tagged gO was also expressed only on the surface of cells cotransfected with gH and gL (data not shown). The level of gB expression on HHV-6B-infected cells was higher than on gB-transfected cells. However, the levels of gH and gQ1 expression on transfected cells were higher than on infected cells (Fig. 1A and B).

We then generated a flow cytometry analysis that used CD46-Ig fusion protein to analyze HHV-6B glycoproteins that bind to CD46 (26). CD46-Ig specifically associated with HHV-6B-infected Molt-3 cells but not mock-infected cells (Fig. 1B). The 293T cells which were transfected with HHV-6 glycoprotein(s) and stained with CD46-Ig showed that CD46-Ig did not bind to cells expressing gH and gL, gB alone, or gH, gL, and gB but did bind to cells transfected with gH, gL, gQ1, and gQ2 (Fig. 1C). Expression of gB did not affect CD46-Ig binding to cells expressing gH, gL, gQ1, and gQ2. These results suggested that CD46 associated with a gH/gL/gQ1/gQ2 complex on the cell surface.

To identify HHV-6 glycoproteins that mediate membrane fusion, we developed a HHV-6 virus-free cell-to-cell fusion assay. 293T effector cells were cotransfected with the plasmids expressing HHV-6B glycoproteins and a plasmid expressing DsRed or were mock transfected. 293T target cells were cotransfected with plasmid expressing CD46 and green fluorescent protein (GFP) (Fig. 2A). Effector cells were cocultured with target cells 24 h after transfection. After coculture for 72 h, the cells were analyzed by fluorescence microscopy. As shown in Fig. 2B, yellow, giant, fused cells were observed when effector cells were cotransfected with plasmids expressing HHV-6B gB, gH, gL, gQ1, and gQ2 and cocultured with CD46-transfected target cells. However, no fused cells were found in the absence of gB.

To quantify fusion efficiency, a dual-luciferase reporter assay was used as previously reported (15). 293T effector cells were cotransfected with plasmid expressing HHV-6B glycoproteins, T7 polymerase (pCAGT7), and *Renilla* luciferase (as an internal control) and cocultured with 293T target cells transfected with CD46 and T7 promoter-driven firefly luciferase (pT7EMCluc) for 72 h. Firefly and *Renilla* luciferase activities were then measured, and fusion efficiency was calculated as described in the Fig. 3 legend. The fusion efficiency of varicella-zoster virus (VZV) envelope glycoproteins was measured as a control (15). Cell-to-cell fusion was 10.2-fold more efficient with gB-, gH-, gL-, gQ1-, and gQ2-transfected effector cells than with mock-transfected effector cells (Fig. 3B). In the absence of gB, gH, gL, gQ1, or gQ2, no significant fusion activity was observed. gO of human cytomegalovirus (HCMV) and HHV-6 have been suggested to form a complex with gH and gL, with the complex being involved in HCMV entry (9, 27). However, transfection with HHV-6B gO did not affect cell-to-cell fusion induced by HHV-6B gB, gH, gL, gQ1, and gQ2 (data not shown). This is in agreement with the previous report that gO is not essential for HCMV cell-to-cell fusion (27). CD46-Ig also bound to HHV-6A (strain GS) gH, gL, gQ1, and gQ2 transfectants (data not shown), and cell-to-cell fusion was observed using HHV-6A envelope glycoproteins (Fig. 3A) (28). Furthermore, cell-to-cell fusion using either HHV-6A or -6B glycoproteins was inhibited by both anti-CD46 and anti-HHV-6A gB MAbs (clone 87-y-13), similar to reports in which syncytium formation by HHV-6A was abrogated by these MAbs (Fig. 4) (29, 30). These

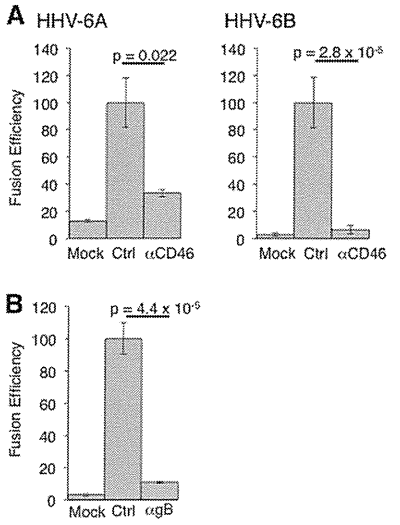

FIG 4 Effect of anti-CD46 and anti-gB MAbs on HHV-6-glycoprotein-mediated cell-to-cell fusion. (A) Cell-to-cell fusion efficiency mediated by HHV-6A and HHV-6B glycoproteins was measured in the presence of anti-CD46 MAb (M75), in the absence of anti-CD46 MAb (Ctrl), and in mock-transfected cells as described in the Fig. 3 legend. Fusion efficiency was calculated as follows: [(firefly luciferase activity/*Renilla* luciferase activity) × 100]/[(firefly luciferase activity/*Renilla* luciferase activity) in control cells]. (B) Cell-to-cell fusion efficiency mediated by HHV-6A glycoproteins was measured in the presence of anti-HHV-6A gB MAb (clone 87-y-13) and in the absence of anti-gB MAb (Ctrl) and in mock-transfected cells as described in the panel A legend. Error bars show the means ± SD of the results determined with quadruplicated samples. The statistical difference was determined by the Student's *t* test. A difference with $P < 0.05$ was considered statistically significant. Data are representative of at least three independent experiments.

results suggested that both HHV-6A and HHV-6B require gB, gH, gL, gQ1, and gQ2 for cell-to-cell fusion.

Cell-to-cell fusion assays were also done *in trans*; i.e., some cells were transfected only with plasmid(s) gB, gH/gL, and/or gQ1/gQ2 and other cells were transfected with plasmids expressing all the other glycoproteins. Little cell-to-cell fusion was observed in *in trans* fusion assays (data not shown). These results suggested that *cis* expression of HHV-6 gB, gH, gL, gQ1, and gQ2 is required for cell-to-cell fusion, unlike that of herpes simplex virus (HSV) and HCMV, in which all the envelope glycoproteins do not need to be expressed on the same cell (17, 31).

This is the first report showing that the HHV-6A and HHV-6B envelope glycoproteins gB, gH, gL, gQ1, and gQ2 are required for cell-to-cell fusion. Herpesviruses enter via two different pathways: (i) direct fusion of the viral envelope with the host cell membrane or (ii) endocytosis followed by fusion between the viral envelope and endosomal membranes (32). Since membrane fusion is needed for herpesvirus entry, our results are consistent with previous reports that anti-gB, -gH, and -gQ1 antibodies block HHV-6 infection (22–24, 33–36). Moreover, our results are also supported by an earlier report that gB and gH are required for polykaryocyte formation after virus infection of permissive cells in cell culture (29). Considering that gBs and gHs of other herpesviruses associate with their respective cellular receptors during viral entry and cell-to-cell fusion (15, 26, 37–41), HHV-6 gB may also mediate viral entry and cell-to-cell fusion by interaction with cellular receptors that are currently unknown in addition to the binding of the gH, gL, gQ1, and gQ2 complex to its receptor CD46. The virus-free HHV-6 fusion assay system developed in this study should help elucidate the HHV-6 entry mechanism.

ACKNOWLEDGMENTS

We thank M. Mastumoto and K. Shida for technical help, Y. Mori (Kobe University) for providing HHV-6A (GS)-infected cells and anti-gH and anti-gB (clone 87-y-13) MAbs, and Y. Matsuura (Osaka University) for providing pCAGT7 and pT7EMCluc.

This work was supported by a Grant-in-Aid for Scientific Research from the Ministry of Education, Science and Culture, Japan (T. Suenaga and H.A.) and in part by grants from the Takeda Science Foundation (T. Suenaga and H.A.).

REFERENCES

1. **Roizmann B, Desrosiers RC, Fleckenstein B, Lopez C, Minson AC, Studdert MJ.** 1992. The family Herpesviridae: an update. The Herpesvirus Study Group of the International Committee on Taxonomy of Viruses. Arch. Virol. **123**:425–449.
2. **Aubin JT, Collandre H, Candotti D, Ingrand D, Rouzioux C, Burgard M, Richard S, Huraux JM, Agut H.** 1991. Several groups among human herpesvirus 6 strains can be distinguished by Southern blotting and polymerase chain reaction. J. Clin. Microbiol. **29**:367–372.
3. **Campadelli-Fiume G, Guerrini S, Liu X, Foa-Tomasi L.** 1993. Monoclonal antibodies to glycoprotein B differentiate human herpesvirus 6 into two clusters, variants A and B. J. Gen. Virol. **74**(Pt 10):2257–2262.
4. **Wyatt LS, Balachandran N, Frenkel N.** 1990. Variations in the replication and antigenic properties of human herpesvirus 6 strains. J. Infect. Dis. **162**:852–857.
5. **Yamanishi K, Okuno T, Shiraki K, Takahashi M, Kondo T, Asano Y, Kurata T.** 1988. Identification of human herpesvirus-6 as a causal agent for exanthem subitum. Lancet **i**:1065–1067.
6. **Asano Y, Yoshikawa T, Suga S, Yazaki T, Kondo K, Yamanishi K.** 1990. Fatal fulminant hepatitis in an infant with human herpesvirus-6 infection. Lancet **335**:862–863.
7. **Clark DA.** 2002. Human herpesvirus 6 and human herpesvirus 7: emerging pathogens in transplant patients. Int. J. Hematol. **76**(Suppl 2):246–252.
8. **Maeki T, Mori Y.** 2012. Features of human herpesvirus-6A and -6B entry. Adv. Virol. **2012**:384069. doi:10.1155/2012/384069.
9. **Mori Y, Akkapaiboon P, Yonemoto S, Koike M, Takemoto M, Sadaoka T, Sasamoto Y, Konishi S, Uchiyama Y, Yamanishi K.** 2004. Discovery of a second form of tripartite complex containing gH-gL of human herpesvirus 6 and observations on CD46. J. Virol. **78**:4609–4616.
10. **Mori Y, Yang X, Akkapaiboon P, Okuno T, Yamanishi K.** 2003. Human herpesvirus 6 variant A glycoprotein H-glycoprotein L-glycoprotein Q complex associates with human CD46. J. Virol. **77**:4992–4999.
11. **Santoro F, Kennedy PE, Locatelli G, Malnati MS, Berger EA, Lusso P.** 1999. CD46 is a cellular receptor for human herpesvirus 6. Cell **99**:817–827.
12. **Chesnokova LS, Nishimura SL, Hutt-Fletcher LM.** 2009. Fusion of epithelial cells by Epstein-Barr virus proteins is triggered by binding of viral glycoproteins gHgL to integrins alphavbeta6 or alphavbeta8. Proc. Natl. Acad. Sci. U. S. A. **106**:20464–20469.
13. **Haan KM, Lee SK, Longnecker R.** 2001. Different functional domains in the cytoplasmic tail of glycoprotein B are involved in Epstein-Barr virus-induced membrane fusion. Virology **290**:106–114.
14. **Pertel PE.** 2002. Human herpesvirus 8 glycoprotein B (gB), gH, and gL can mediate cell fusion. J. Virol. **76**:4390–4400.
15. **Suenaga T, Satoh T, Somboonthum P, Kawaguchi Y, Mori Y, Arase H.** 2010. Myelin-associated glycoprotein mediates membrane fusion and entry of neurotropic herpesviruses. Proc. Natl. Acad. Sci. U. S. A. **107**:866–871.
16. **Turner A, Bruun B, Minson T, Browne H.** 1998. Glycoproteins gB, gD, and gHgL of herpes simplex virus type 1 are necessary and sufficient to mediate membrane fusion in a Cos cell transfection system. J. Virol. **72**:873–875.
17. **Vanarsdall AL, Ryckman BJ, Chase MC, Johnson DC.** 2008. Human cytomegalovirus glycoproteins gB and gH/gL mediate epithelial cell-cell fusion when expressed either in cis or in trans. J. Virol. **82**:11837–11850.
18. **Chowdary TK, Cairns TM, Atanasiu D, Cohen GH, Eisenberg RJ,**

Heldwein EE. 2010. Crystal structure of the conserved herpesvirus fusion regulator complex gH-gL. Nat. Struct. Mol. Biol. 17:882–888.
19. Eisenberg RJ, Atanasiu D, Cairns TM, Gallagher JR, Krummenacher C, Cohen GH. 2012. Herpes virus fusion and entry: a story with many characters. Viruses 4:800–832.
20. Heldwein EE, Lou H, Bender FC, Cohen GH, Eisenberg RJ, Harrison SC. 2006. Crystal structure of glycoprotein B from herpes simplex virus 1. Science 313:217–220.
21. Matsuura H, Kirschner AN, Longnecker R, Jardetzky TS. 2010. Crystal structure of the Epstein-Barr virus (EBV) glycoprotein H/glycoprotein L (gH/gL) complex. Proc. Natl. Acad. Sci. U. S. A. 107:22641–22646.
22. Foà-Tomasi L, Guerrini S, Huang T, Campadelli-Fiume G. 1992. Characterization of human herpesvirus-6(U1102) and (GS) gp112 and identification of the Z29-specified homolog. Virology 191:511–516.
23. Takeda K, Okuno T, Isegawa Y, Yamanishi K. 1996. Identification of a variant A-specific neutralizing epitope on glycoprotein B (gB) of human herpesvirus-6 (HHV-6). Virology 222:176–183.
24. Kawabata A, Oyaizu H, Maeki T, Tang H, Yamanishi K, Mori Y. 2011. Analysis of a neutralizing antibody for human herpesvirus 6B reveals a role for glycoprotein Q1 in viral entry. J. Virol. 85:12962–12971.
25. Tang H, Hayashi M, Maeki T, Yamanishi K, Mori Y. 2011. Human herpesvirus 6 glycoprotein complex formation is required for folding and trafficking of the gH/gL/gQ1/gQ2 complex and its cellular receptor binding. J. Virol. 85:11121–11130.
26. Satoh T, Arii J, Suenaga T, Wang J, Kogure A, Uehori J, Arase N, Shiratori I, Tanaka S, Kawaguchi Y, Spear PG, Lanier LL, Arase H. 2008. PILRalpha is a herpes simplex virus-1 entry coreceptor that associates with glycoprotein B. Cell 132:935–944.
27. Vanarsdall AL, Chase MC, Johnson DC. 2011. Human cytomegalovirus glycoprotein gO complexes with gH/gL, promoting interference with viral entry into human fibroblasts but not entry into epithelial cells. J. Virol. 85:11638–11645.
28. Akkapaiboon P, Mori Y, Sadaoka T, Yonemoto S, Yamanishi K. 2004. Intracellular processing of human herpesvirus 6 glycoproteins Q1 and Q2 into tetrameric complexes expressed on the viral envelope. J. Virol. 78:7969–7983.
29. Mori Y, Seya T, Huang HL, Akkapaiboon P, Dhepakson P, Yamanishi K. 2002. Human herpesvirus 6 variant A but not variant B induces fusion from without in a variety of human cells through a human herpesvirus 6 entry receptor, CD46. J. Virol. 76:6750–6761.
30. Seya T, Hara T, Matsumoto M, Akedo H. 1990. Quantitative analysis of membrane cofactor protein (MCP) of complement. High expression of MCP on human leukemia cell lines, which is down-regulated during cell differentiation. J. Immunol. 145:238–245.
31. Atanasiu D, Saw WT, Cohen GH, Eisenberg RJ. 2010. Cascade of events governing cell-cell fusion induced by herpes simplex virus glycoproteins gD, gH/gL, and gB. J. Virol. 84:12292–12299.
32. Connolly SA, Jackson JO, Jardetzky TS, Longnecker R. 2011. Fusing structure and function: a structural view of the herpesvirus entry machinery. Nat. Rev. Microbiol. 9:369–381.
33. Liu DX, Gompels UA, Foa-Tomasi L, Campadelli-Fiume G. 1993. Human herpesvirus-6 glycoprotein H and L homologs are components of the gp100 complex and the gH external domain is the target for neutralizing monoclonal antibodies. Virology 197:12–22.
34. Okuno T, Sao H, Asada H, Shiraki K, Takahashi M, Yamanishi K. 1990. Analysis of a glycoprotein of human herpesvirus 6 (HHV-6) using monoclonal antibodies. Virology 176:625–628.
35. Qian G, Wood C, Chandran B. 1993. Identification and characterization of glycoprotein gH of human herpesvirus-6. Virology 194:380–386.
36. Takeda K, Haque M, Sunagawa T, Okuno T, Isegawa Y, Yamanishi K. 1997. Identification of a variant B-specific neutralizing epitope on glycoprotein H of human herpesvirus-6. J. Gen. Virol. 78(Pt 9):2171–2178.
37. Akula SM, Pramod NP, Wang FZ, Chandran B. 2002. Integrin alpha3beta1 (CD 49c/29) is a cellular receptor for Kaposi's sarcoma-associated herpesvirus (KSHV/HHV-8) entry into the target cells. Cell 108:407–419.
38. Arii J, Goto H, Suenaga T, Oyama M, Kozuka-Hata H, Imai T, Minowa A, Akashi H, Arase H, Kawaoka Y, Kawaguchi Y. 2010. Non-muscle myosin IIA is a functional entry receptor for herpes simplex virus-1. Nature 467:859–862.
39. Feire AL, Roy RM, Manley K, Compton T. 2010. The glycoprotein B disintegrin-like domain binds beta 1 integrin to mediate cytomegalovirus entry. J. Virol. 84:10026–10037.
40. Soroceanu L, Akhavan A, Cobbs CS. 2008. Platelet-derived growth factor-alpha receptor activation is required for human cytomegalovirus infection. Nature 455:391–395.
41. Wang X, Huong SM, Chiu ML, Raab-Traub N, Huang ES. 2003. Epidermal growth factor receptor is a cellular receptor for human cytomegalovirus. Nature 424:456–461.

nature COMMUNICATIONS

ARTICLE

Received 24 Sep 2012 | Accepted 10 Apr 2013 | Published 14 May 2013

DOI: 10.1038/ncomms2857

Toll-like receptor 3 recognizes incomplete stem structures in single-stranded viral RNA

Megumi Tatematsu[1], Fumiko Nishikawa[2], Tsukasa Seya[1] & Misako Matsumoto[1]

Endosomal Toll-like receptor 3 (TLR3) serves as a sensor of viral infection and sterile tissue necrosis. Although TLR3 recognizes double-stranded RNA, little is known about structural features of virus- or host-derived RNAs that activate TLR3 in infection/inflammatory states. Here we demonstrate that poliovirus-derived single-stranded RNA segments harbouring stem structures with bulge/internal loops are potent TLR3 agonists. Functional poliovirus-RNAs are resistant to degradation and efficiently induce interferon-α/β and proinflammatory cytokines in human and mouse cells in a TLR3-dependent manner. The N- and C-terminal double-stranded RNA-binding sites of TLR3 are required for poliovirus-RNA-mediated TLR3 activation. Like polyriboinosinic:polyribocytidylic acid, a synthetic double-stranded RNA, these RNAs are internalized into cells via raftlin-mediated endocytosis and colocalized with TLR3. Raftlin-associated RNA uptake machinery and the TLR3 RNA-sensing system appear to recognize an appropriate topology of multiple RNA duplexes in poliovirus-RNAs. Hence, TLR3 is a sensor of extracellular viral/host RNA with stable stem structures derived from infection or inflammation-damaged cells.

[1] Department of Microbiology and Immunology, Hokkaido University Graduate School of Medicine, Kita 15, Nishi 7, Kita-ku, Sapporo 060-8638, Japan. [2] Biomedical Research Institute, National Institute of Advanced Industrial Science and Technology (AIST), Tsukuba 305-8566, Japan. Correspondence and requests for materials should be addressed to M.M. (email: matumoto@pop.med.hokudai.ac.jp).

Type I interferon (IFN) production is crucial for controlling virus infections[1,2]. Toll-like receptors (TLRs) 3, 7, 8 and 9 and RIG-I-like receptors detect viral nucleic acids in the endosomes and cytoplasm, respectively, and induce cytokine production, including type I IFNs (IFN-α and IFN-β), via distinct adaptor proteins[3]. TLR3 recognizes double-stranded RNA (dsRNA), a viral replication intermediate that is produced by positive-strand RNA viruses and DNA viruses, and signals to produce IFN-β and proinflammatory cytokines through the Toll-interleukin-1 (IL-1) receptor domain-containing adaptor molecule-1 (TICAM-1, also known as TRIF)[4–8]. TLR3 is expressed at high levels in myeloid dendritic cells (DCs), especially in professional antigen-presenting DCs, such as mouse splenic CD8α$^+$ DCs and human CD141$^+$ DCs, and localizes to the early endosome[9–11]. Although macrophages, fibroblasts and epithelial cells also express TLR3 on the cell surface as well as the endosomal membrane, TLR3-mediated signalling initiates from the endosomal compartment[12]. Thus, TLR3 activation depends on the uptake of extracellular virus-derived RNA molecules.

Studies using TLR3-deficient mice demonstrated that TLR3 mediates a protective response against positive-strand RNA virus infection, including coxsackie virus group B serotype 3, encephalomyocarditis virus and poliovirus (PV), all of which belong to the *Picornaviridae* family[13–16]. TLR3- or TICAM-1-deficient human PV receptor (PVR)-transgenic mice were more susceptible than normal PVR-transgenic mice to intraperitoneal or intravenous inoculation with a low titre of PV[15,16]. TLR3-dependent type I IFN production by splenic CD11c$^+$ DCs and macrophages was essential for the protection of PVR-transgenic mice against PV infection. In addition to mouse studies, genetic studies in the patients with herpes simplex encephalitis demonstrated that the TLR3-TICAM-1 pathway is involved in the protection against herpes simplex virus-1 encephalitis in children[17–19]. Collectively, these findings indicate that TLR3 has an important role in antiviral responses in both humans and mice. However, several studies have also demonstrated that TLR3-mediated signalling exacerbates RNA virus infection including West Nile virus (positive-strand RNA virus), influenza virus and phelebovirus (negative-strand RNA viruses)[20–22]. TLR3-dependent inflammatory cytokine and chemokine productions have an impact on virus-induced pathology and host survival, and, remarkably, RNA from necrotic cells or host mRNA are also recognized by TLR3[23,24]. However, RNA species detected by TLR3 have not been analysed and little is known about the essential structural elements of virus- or host-derived RNAs capable of activating TLR3 in an infection/inflammatory state.

In the current study, we analysed the RNA structure recognized by TLR3 using *in vitro*-transcribed RNAs derived from PV. We found that, in addition to dsRNA, PV-derived structured RNAs harbouring ds regions with bulges and internal loops are potent TLR3 ligands. The PV-RNAs activated endosomal TLR3 in mouse and human cells, leading to the production of IFN-α/β and proinflammatory cytokines.

Results

Identification of RNA structures recognized by TLR3. To examine whether viral RNA activates TLR3 extracellularly, mouse splenic DCs from wild-type (WT) or TLR3-deficient mice were stimulated with total RNA isolated from PV-infected or uninfected Vero cells, or a synthetic viral dsRNA analogue, polyriboinosinic:polyribocytidylic acid (poly(I:C)), in FCS-free medium. Poly(I:C) induced type I IFN production by mouse splenic DCs in a TLR3-independent manner (Fig. 1a). The results reflect a current notion that cytosolic RNA helicase, melanoma differentiation-associated gene 5 (MDA5), in addition to endosomal TLR3, senses poly(I:C) to induce type I IFNs in mouse DCs[25]. However, this is not the case in RNA from PV-infected cells, which induces type I IFNs and proinflammatory cytokines in splenic DCs largely through their TLR3 (Fig. 1a and Supplementary Fig. S1). Notably, RNA from PV-uninfected cells had no potential for IFN/cytokine induction (Fig. 1a and Supplementary Fig. S1). Given that PV infection leads to a rapid inhibition of host-cell RNA synthesis[26], the main RNA species in PV-infected Vero cells were approximately 8,000-nucleotide (nt) RNA corresponding to the PV genome and its replicative form, which were segmented into approximately 1,000–2,000-nt RNAs in the FCS-free culture medium (Fig. 1b). The ~8,000-nt PV-RNAs were degraded by treatment with single-stranded RNA (ssRNA)- and dsRNA-specific RNase, suggesting the existence of ss and ds forms of PV-derived RNAs in PV-infected cells (Supplementary Fig. S2).

A functional screening for PV-derived ssRNA and dsRNA was performed using an IFN-β promoter reporter assay to determine the RNA structure recognized by TLR3. Approximately 540–920 nts contiguous sense (PV1–10) or complementary (cPV1–10) RNAs and their dsRNA forms (dsPV1–10) were transcribed *in vitro* using PV-cDNA as a template (Fig. 1c and Supplementary Table S1), and their TLR3-activating ability was assessed. HEK293 cells transfected with the TLR3-expression vector or empty vector, together with the IFN-β promoter reporter plasmid, were stimulated with PV-RNAs in FCS-free or FCS-containing media. All PV-derived dsRNAs induced TLR3-dependent IFN-β promoter activation similar to poly(I:C) (Fig. 1d, left panel). Interestingly, several PV-ssRNAs, either sense or complementary RNA, also activated the IFN-β promoter through TLR3 in FCS-free medium (Fig. 1d, centre and right panels). We further examined the effect of FCS on the IFN-β-inducing abilities of PV-RNAs using PV5. PV5 retained TLR3-activating ability, even in the FCS-containing medium (Fig. 1e).

To explore the relationship between TLR3-activating capacity and the degradability of PV-RNAs, PV-RNAs were incubated in FCS(−) or FCS(+) medium for 30 min at 37 °C and then subjected to agarose gel electrophoresis. Non-functional PV-RNAs were readily degraded in the FCS(−) or FCS(+) medium, whereas functional RNAs, including high-potential PV5 and cPV5 and low-potential PV6, were stable before and after incubation in the FCS(+) medium (Fig. 2a). Correspondingly, dose-dependent TLR3 activation was observed with PV5 and PV6 but not with others including cPV1 (Fig. 2b). Notably, these PV-RNAs stimulated the cytosolic RNA sensors when transfected into cells (Supplementary Fig. S3a). TLR3-mediated IFN-β promoter activation was also observed with PV5- or cPV5-containing long-size PV-RNAs, although the activity was less than that of PV5 (Supplementary Fig. S3b and Supplementary Table S1). In addition, segmentation of PV5 into three ~200-nt RNAs (PV5 a, b and c) destroyed the activity of intact PV5, despite the fact that these RNA segments were resistant to degradation (Supplementary Fig. S3c and Supplementary Table S1). These results suggested that an appropriate length of PV-RNAs with a stable structure activate endosomal TLR3, inducing IFN-β promoter activation.

PV-RNAs induce IFN-β production by human fibroblasts. We next examined whether PV-RNAs induced IFN-β production from human fibroblasts and epithelial cells that endogenously expressed TLR3. MRC5 cells were stimulated with cPV1, PV5, PV6 or dsPV5 extracellulary, and IFN-β mRNA was assessed using quantitative PCR (qPCR). PV5 and PV6 induced IFN-β mRNA expression in MRC5 cells similar to dsPV5 stimulation

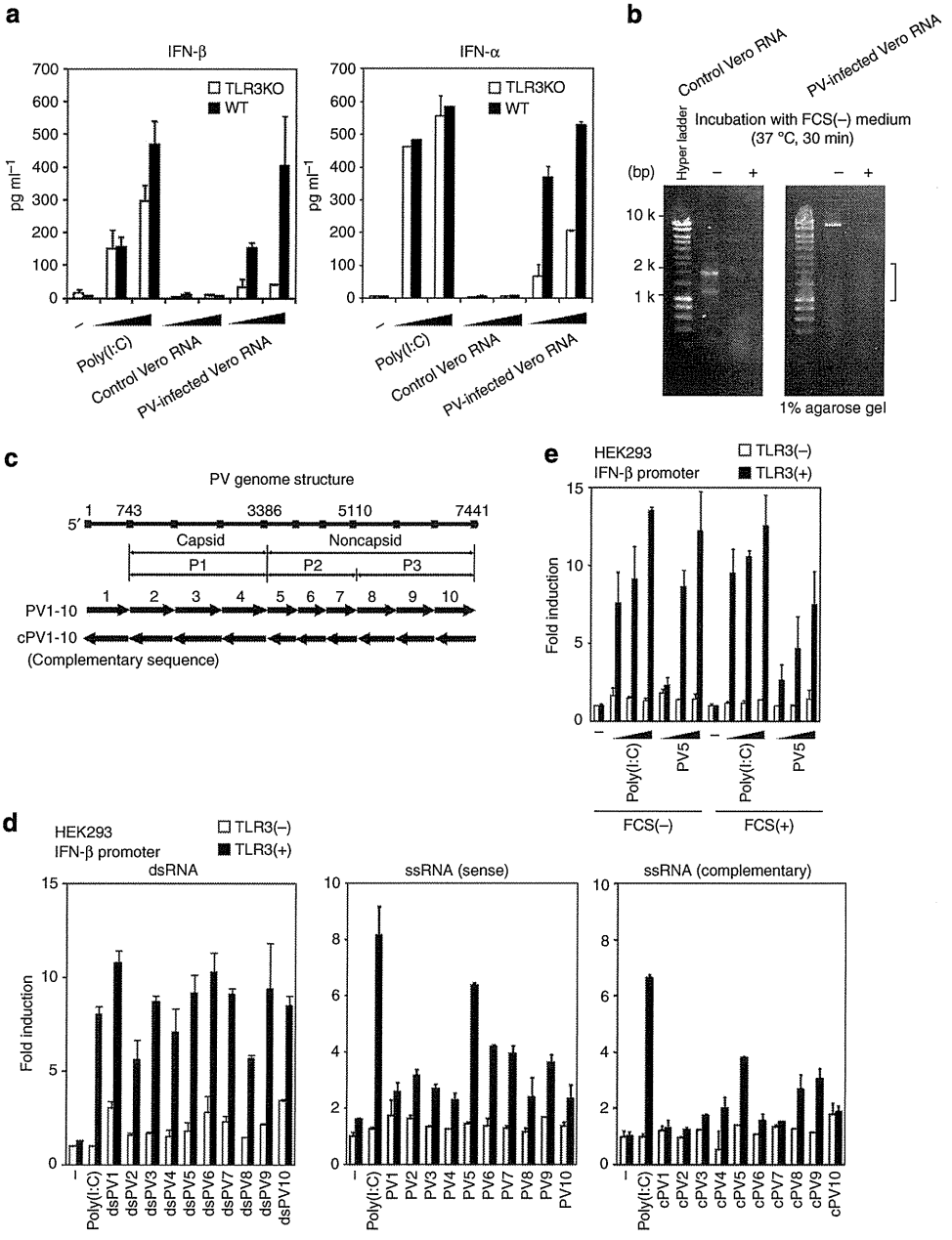

Figure 1 | Extracellular PV-RNAs induce TLR3-mediated type I IFN production. (**a**) Mouse splenic CD11c$^+$ DCs from WT or TLR3$^{-/-}$ mice (1×10^6 per ml) were stimulated with medium alone (–), poly(I:C), total RNA from PV-infected Vero cells or total RNA from uninfected Vero cells (25, 100 μg ml^{-1}) for 24 h in FCS(–) AIM-V medium. RNAs were pre-treated with polymyxin B (5 μg ml^{-1}) for 1 h before addition. IFN-α/β levels in culture supernatants were measured using ELISA. Representative data from three independent experiments are shown (mean ± s.d.). (**b**) The RNA extracted from PV-infected or uninfected Vero cells was incubated in FCS(–) AIM-V medium for 30 min and then electrophoresed on a 1% agarose gel. The PV-RNAs were segmented into approximately 1,000–2,000-nt RNAs in FCS-free medium (right panel, square bracket). (**c**) Constructs of *in vitro*-transcribed PV-RNAs. Diagram of PV genome is shown (Top). Coding regions for viral capsid proteins (P1) and noncapsid proteins (P2 and P3) are indicated. Positions of the sense RNAs (PV1-10) and the complementary RNAs (cPV1-10) corresponding to the PV genome are shown as arrows. Each starting and ending position and length are described in Supplementary Table S1. (**d**) PV-RNA-induced TLR3-mediated IFN-β promoter activation. HEK293 cells were transfected with an empty vector (–) or expression plasmid for TLR3, together with the IFN-β promoter reporter and phRL-TK. Twenty-four hours after transfection, culture media was removed and 10 μg ml^{-1} poly(I:C), PV-derived dsRNAs, dsPV1-dsPV10 (left panel), sense RNAs, PV1-PV10 (middle panel) or complementary RNAs, cPV1-cPV10 (right panel), were added with FCS-free medium. Luciferase activity was measured 6 h after stimulation and shown as mean fold index induction compared with non-stimulated cells. Representative data from three independent experiments are shown (mean ± s.d.). (**e**) Effect of FCS on the PV5-induced TLR3-mediated IFN-β promoter activation. Cells were stimulated with increasing amounts of poly(I:C) or PV5 (2.5, 10 or 25 μg ml^{-1}) in the condition of FCS-free or -containing medium.

(Fig. 2c). mRNA encoding the proinflammatory cytokines, IL-6 and TNF-α, were also induced by PV5, PV6 or dsPV5. Similarly, HeLa cells greatly increased IFN-β mRNA expression in response to PV5, PV6 or dsPV5 (Fig. 2d). In contrast, cPV1 did not induce any cytokine mRNA transcription from MRC5 and HeLa cells.

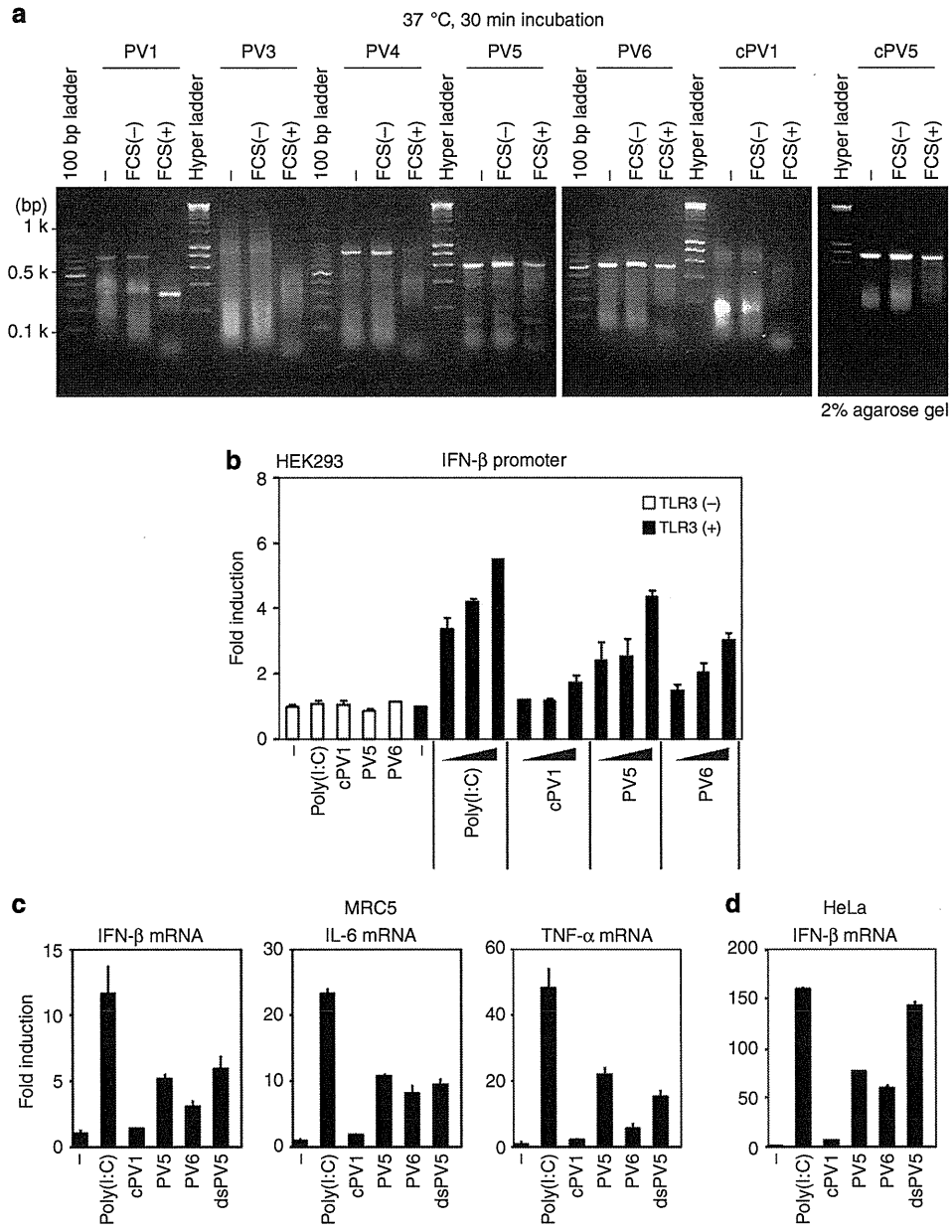

Figure 2 | PV-ssRNA-induced TLR3 activation is correlated with the degradability of RNAs. (**a**) PV-RNAs were incubated in cell-free FCS-free or -containing medium at 37 °C. Non-treated RNA or RNA incubated for 30 min were loaded onto a 2% agarose gel. (**b**) HEK293 cells transiently expressing TLR3 were stimulated with increasing amounts of poly(I:C), cPV1, PV5 or PV6 (2.5, 10 or 25 μg ml^{-1}) for 6 h. HEK293 cells transfected with empty vector were stimulated with 25 μg ml^{-1} poly(I:C) or indicated PV-RNA. IFN-β promoter activation is shown as mean fold index induction compared with non-stimulated cells. Representative data from three independent experiments are shown. (**c**,**d**) IFN-β mRNA expression induced by PV-RNAs in human cells expressing TLR3. MRC5 cells (**c**) or HeLa cells (**d**) in FCS(−) AIM-V medium were stimulated with 20 μg ml^{-1} poly(I:C) or PV-derived RNAs for 3 h. Total RNA was extracted and quantitative PCR was performed using primers for the respective genes. Expression of each gene was normalized to glyceraldehyde 3-phosphate dehydrogenase mRNA expression. Data are shown as the mean ± s.d. Representative data from three independent experiments are shown.

TLR3 recognizes PV-RNA through the dsRNA-binding sites. Biochemical studies using *in vitro*-transcribed dsRNAs have shown that relatively long stretches of dsRNA (>90 bp in length) are required for TLR3-mediated IFN-β promoter activation in HEK293/TLR3 cells and cytokine production from mouse myeloid DCs[11,27]. To determine the structural features of TLR3-activating or non-activating RNAs, the secondary structure of PV-RNAs was predicted using the mfold WebServer program, which calculates the minimum free-energy secondary structure[28]. Each PV-RNA contains ds (<11 bp in length) and ss regions, and, intriguingly, the percentages of stem/loop structure were almost the same in each PV-RNA (Fig. 3a). However, the secondary structure models of cPV1, PV5 and PV6 have clearly showed that cPV1 contains multiple branched stems and large loop structures that may be targeted by RNases, whereas functional PV5 and PV6 possess tandemly arranged ds regions, which were segmented with bulge or internal loops. Thus, RNAs that we prepared are not a typical ds structure of the TLR3 ligand. The topology of multiple dsRNA regions and the overall secondary and tertiary structures of PV-RNAs appear to influence the stability and TLR3-activating ability.

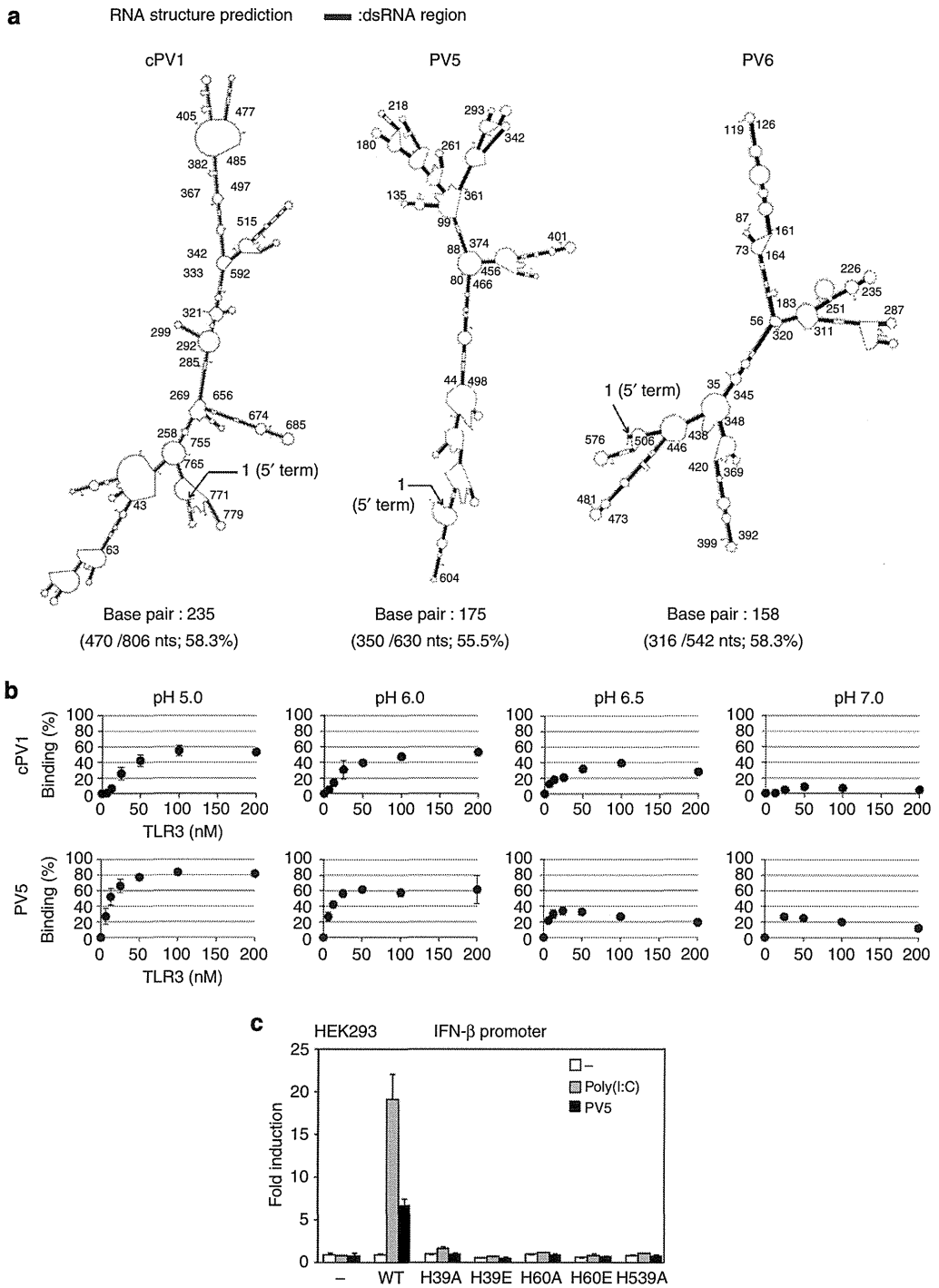

Figure 3 | Both N- and C-terminal dsRNA-binding sites of TLR3 are required for PV-RNA-induced TLR3 activation. (**a**) Secondary structure of PV-RNAs (cPV1, PV5 and PV6) predicted by the mfold software. Thick lines indicate dsRNA regions (1-11 bp). The starting and ending positions of ds regions are shown with the nt number. A total number of base pair and the number of nts involved in base pairing in cPV1, PV5 and PV6 are described under the secondary-structure model. (**b**) Binding affinity of PV-RNAs to TLR3 ECD under different pH conditions. ^{32}P-labelled PV-RNAs (cPV1 and PV5) were mixed with varying concentrations of hTLR3 ECD protein and passed through a nitrocellulose filter. After washing, bound radioactivity was measured, and binding activities were calculated as a percentage of input RNA before filtration. The apparent dissociation constant (Kd) values calculated for cPV1 and PV5 were 39 ± 16 and 10 ± 3 nM (pH 5.0), and 31 ± 13 and 7 ± 3 nM (pH 6.0), respectively. (**c**) HEK293 cells were transfected with an empty vector or expression plasmid for WT TLR3 or each TLR3 mutant (H39A, H39E, H60A, H60E and H539A), together with the IFN-β promoter reporter plasmid and phRL-TK. Twenty-four hours post transfection, cells were stimulated with 10 μg ml^{-1} poly(I:C) or PV5 in FCS-free medium. Luciferase activity was measured 6 h after stimulation. Representative data from three independent experiments are shown.

We then tested the binding ability of intact PV5 and cPV1 to the recombinant TLR3 ectodomain (ECD) protein under the various pH conditions using a filter binding assay[29]. The ability of PV5 to bind TLR3 was higher than cPV1 at low concentrations of TLR3 ECD in an acidic environment (pH 5.0 and 6.0) (Fig. 3b). Even in a neutral pH (7.0), PV5 weakly bound to TLR3 ECD,

whereas cPV1 remained unbound (Fig. 3b). The binding of PV-RNAs to TLR3 ECD was specific because unlabelled PV5 inhibited the ^{32}P-labelled PV5 binding dose-dependently. In addition, dsDNA (200 bp in length) hardly bound to TLR3 ECD under any pH condition (Supplementary Fig. S4).

TLR3 ECD is composed of 23 leucine-rich repeats (LRRs) and the N- and C-terminal flanking regions[30]. Structural analysis of mouse TLR3 ECD–dsRNA complex revealed that TLR3 ECD dimerized on 46-bp dsRNA[31]. dsRNA interacted with both an N- and C-terminal-binding site on the glycan-free surface of each TLR3 ECD, which are on opposite sides of the dsRNA. The point mutation analyses of human/mouse TLR3 demonstrated that H539 and N541 located in LRR20, H39 in LRR-NT and H60 in LRR1 form the C- and N-terminal-binding site, and are essential for dsRNA-induced TLR3-mediated signalling[29,32]. We therefore investigated whether PV5, like dsRNA, activates TLR3 through interaction with the N- and C-terminal-binding sites of TLR3. When TLR3 mutants, in which H39, H60 or H539 was substituted with Ala or Glu, were expressed in HEK293 cells, PV5 failed to induce IFN-β promoter activation, similar to poly(I:C) (Fig. 3c). Thus, PV5 appears to interact with the N- and C-terminal dsRNA-binding sites of TLR3 and oligomerize the receptor, leading to the activation of downstream signalling molecules. However, we cannot rule out the possibility that amino acids of the TLR3 ECD, irrelevant to the direct dsRNA binding, participate in the interaction with PV-RNAs.

PV5 is internalized and colocalizes with endosomal TLR3. TLR3 activation by poly(I:C) requires clathrin-mediated internalization of extracellular poly(I:C)[33]. In human myeloid DCs and epithelial cells such as HeLa cells, the cytoplasmic raft protein, raftlin, induces poly(I:C) uptake through interaction with clathrin–AP-2 complex[34,35]. To understand how extracellular PV-RNAs activate endosomal TLR3, we examined the requirement of raftlin in PV-RNA-induced TLR3 activation by gene silencing of raftlin with small interfering RNA (siRNA). PV-ssRNA or -dsRNA-induced IFN-β promoter activation was greatly decreased when raftlin was knocked down in HEK293 cells, similar to what was observed with poly(I:C) stimulation (Fig. 4a). Furthermore, raftlin-knockdown HeLa cells were also impaired in their ability to induce the expression of IFN-β mRNA in response to PV5 (Fig. 4b). Again, TICAM-1 was essential for PV-RNA-induced signalling (Fig. 4a).

Immunofluorescent analyses demonstrated that surface-bound Cy3-labelled PV5 was internalized within a 5-min incubation at 37 °C. PV5 colocalized with TLR3 and the early endosome marker, EEA1, after 15 min, and this was sustained for up to 60 min (Fig. 4c). In contrast, co-localization of Cy3-PV5 with LAMP1, a late endosome/lysosome marker, was observed after incubation for 30 min (Fig. 4c). The internalization of PV5 was similar to that of poly(I:C)[35]. Indeed, PV5 activity was inhibited by the pre-treatment of cells with B-type CpG oligodeoxynucleotide (ODN), which shares an uptake receptor with poly(I:C) (Supplementary Fig. S5). Taken together, these results strongly suggest that functional PV-RNAs use the poly(I:C)/ODN-uptake receptor for raftlin-mediated endocytosis and that long-term retention of PV5 in the early endosome allows TLR3 to oligomerize for IFN-β production in human cells.

PV-RNAs induce TLR3-dependent IFN production by mouse DCs. To show the TLR3 dependency in PV-RNA-induced cellular responses, mouse macrophages and DCs from WT or TLR3-deficient mice were used for cytokine assay. When bone marrow-derived macrophages from WT mice were stimulated with cPV1, PV5, PV6 or dsPV5 in the FCS-containing medium, they produced IFN-β in response to PV5, PV6 or dsPV5 (Supplementary Fig. S6). Similarly, splenic CD11c$^+$ DCs produced significant amounts of IFN-α/β, TNF-α and IL-6 in response to PV5, PV6 or dsPV5 in the FCS-containing medium (Fig. 5a). The activity of PV-RNAs were augmented in FCS-free medium (Supplementary Fig. S7). Unlike human fibroblasts and epithelial cells, mouse CD11c$^+$ DCs produced cytokines in response to cPV1 with or without FCS in the media, although the levels were relatively low compared with those induced by exposure to PV5, PV6 or dsPV5. Notably, PV-RNA-induced cytokine production was absent from TLR3-deficient DCs (Fig. 5a). Remarkably, cPV1 induced substantial production of proinflmmatory cytokines in FCS-free medium by mouse splenic CD8α$^+$ DCs, expressing a high level of TLR3 in a TLR3-dependent manner, similar to cells cultured with PV5, PV6 or dsPV5 (Supplementary Fig. S8). One possible interpretation of these results is that intact cPV1 possesses TLR3-activating ability and that CD11c$^+$ or CD8α$^+$ DCs promptly take up intact cPV1 before being degraded in FCS-free or -containing medium and deliver it to the endosomal compartment where TLR3 resides. Indeed, intact cPV1 bound to the TLR3 ECD under acidic conditions, though with lower affinity than PV5 (Fig. 3b). When PV5 was pre-treated with RNaseIII, a dsRNA-specific RNase, cytokine production by splenic CD11c$^+$ DCs was abrogated, indicating that RNA duplex is required for PV5-induced TLR3 activation (Fig. 5b).

The estimated secondary-structure model of PV5. To clarify the secondary structure of PV5, we performed the partial digestion of PV5 using MazF at room temperature. MazF is an ACA-specific endoribonuclease that specifically cleaves ssRNA regions at the 5′-end of the ACA sequence, but not dsRNA regions[36]. Cleavage occurs at the 5′ end of the first A residue in an ACA sequence, which produces 2′,3′-cyclic phosphate and the other 5′ OH group[37]. There are 12 ACA sites in PV5. Therefore, to estimate the size of cleaved fragments, PV5-deletion mutants were also digested with MazF (Fig. 6a). Comparison of the cleaved fragments with the mutant RNAs clearly demonstrated that the 124 ACA site in PV5, which was expected to be a dsRNA region, was resistant to cleavage (Fig. 6b). At approximately the 40-mer RNA position, two fragments were detected in PV5(456)/MazF and PV5/MazF. The slow-migration band intensity increased in a time-dependent manner and the fast-migration band intensity gradually decreased. This indicated that the former may be the final digested fragment and the latter was at an intermediate stage of digestion. This was confirmed by additional digestion analyses (Supplementary Fig. S9). We compared our data with several secondary-structure models (RNAfold, mfold and centroidfold) of PV5 and determined that the mfold secondary-structure model was most fitted among them (Fig. 6b and Supplementary Fig. S10).

The core RNA structure required for TLR3 activation. Based on the mfold model, we attempted to identify the core RNA structure required for TLR3 activation in PV5. PV5-derived RNAs partly having PV5 secondary structure (PV5-D1–PV5-D5) were made by *in vitro* transcription (Fig. 7a), and their stability and TLR3-activating ability were assessed. PV5-D1, D3 and D5 were resistant to degradation, and extracellularly activate TLR3 similar to PV5, leading to IFN-β promoter activation in HEK293 cells and cytokine production in mouse splenic DCs or bone marrow-derived macrophages (Fig. 7b–d). In contrast, PV5-D2 and -D4, which were resistant to degradation in FCS-free medium but were readily degraded in FCS-containing medium,

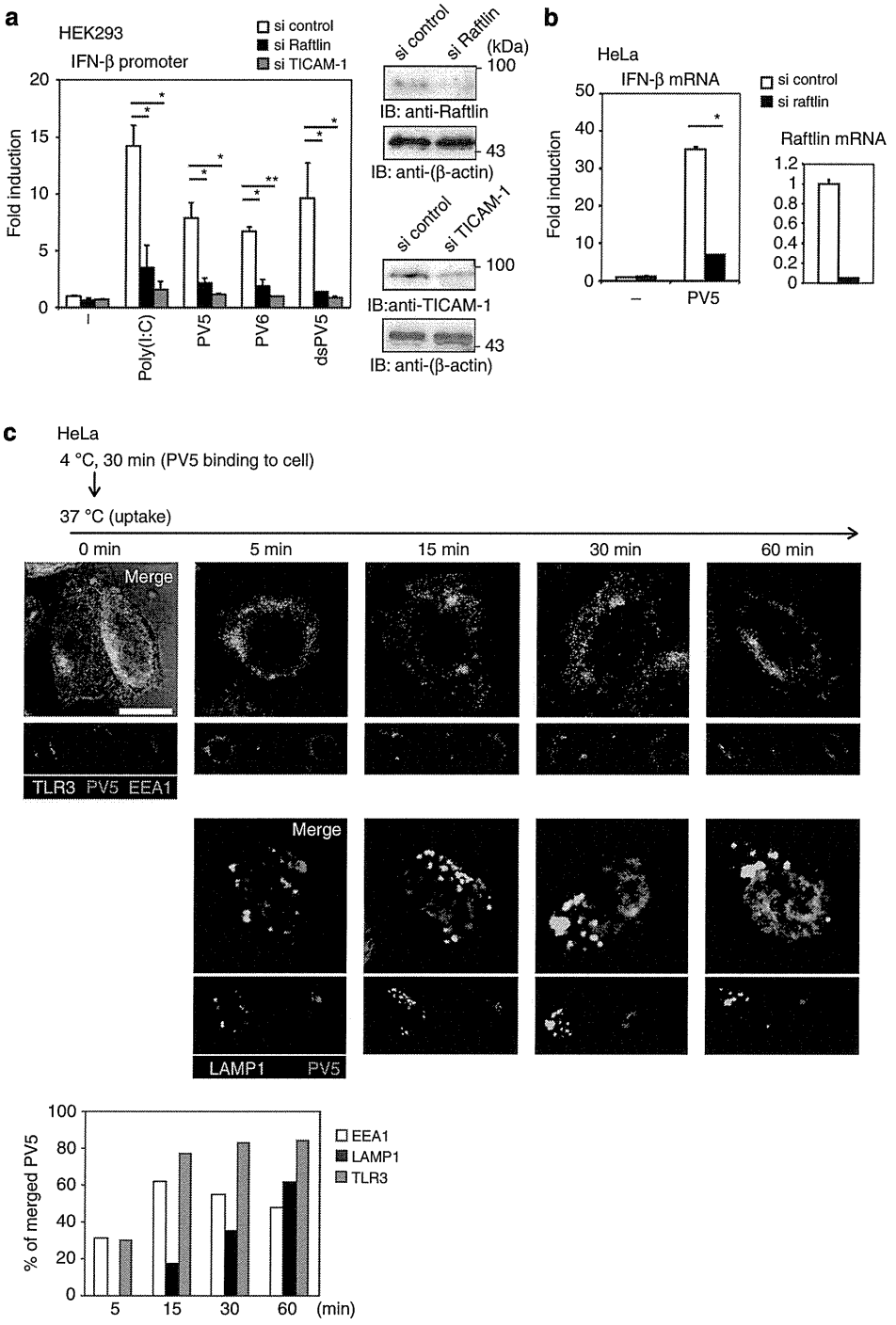

Figure 4 | Raftlin-mediated endocytosis is essential for PV-RNA-induced IFN-β production by human cells. (**a**) Left panels: HEK293 cells were transfected with control, raftlin or TICAM-1 siRNAs (20 pmol), together with the expression vector for human TLR3 and the IFN-β reporter plasmid. Forty-eight hours after transfection, cells were washed and stimulated with 20 μg ml^{-1} poly(I:C) or PV-RNAs. After 6 h, luciferase reporter activity was measured and expressed as the fold induction relative to the activity of unstimulated cells. Representative data from three independent experiments are shown (mean ± s.d.). Student's *t*-test was used for statistical analysis. *$P<0.05$ and **$P<0.01$. Right panels: Knockdown of raftlin or TICAM-1 was confirmed using western blotting. (**b**) HeLa cells were transfected with the control or raftlin siRNAs. Forty-eight hours after transfection, cells were washed and stimulated with 20 μg ml^{-1} PV5 for 3 h. Total RNA was extracted, and quantitative PCR was performed using primers for the IFN-β and raftlin genes. Expression of genes was normalized to glyceraldehyde 3-phosphate dehydrogenase mRNA expression. Data are shown as the mean ± s.d. Representative data from three independent experiments are shown. *$P<0.05$. (**c**) HeLa cells were incubated with 15 μg ml^{-1} Cy3-PV5 for 30 min at 4 °C. After washing, cells were incubated for up to 60 min at 37 °C. At timed intervals, cells were fixed and permeabilized. After staining with anti-TLR3 mAb and anti-EEA1 pAb (upper panels) or anti-LAMP1 mAb (lower panels), cells were incubated with an Alexa Fluor-488- or -633-conjugated secondary Ab and then analysed using confocal microscopy. Red, Cy3-PV5; green, TLR3 or LAMP1; blue, EEA1; light blue, nuclei with 4′,6-diamidino-2-phenylindole; white, merged PV5 with TLR3 and EEA1; and yellow, merged PV5 with LAMP1. Scale bar, 10 μm. Co-localization between PV5 and TLR3, EEA1 or LAMP1 was analysed by counting the merged PV5 spots with each molecule in 70 PV5-internalizing cells. The data are shown as % of merged PV5 with EEA1, LAMP1 or TLR3 at indicated time points.

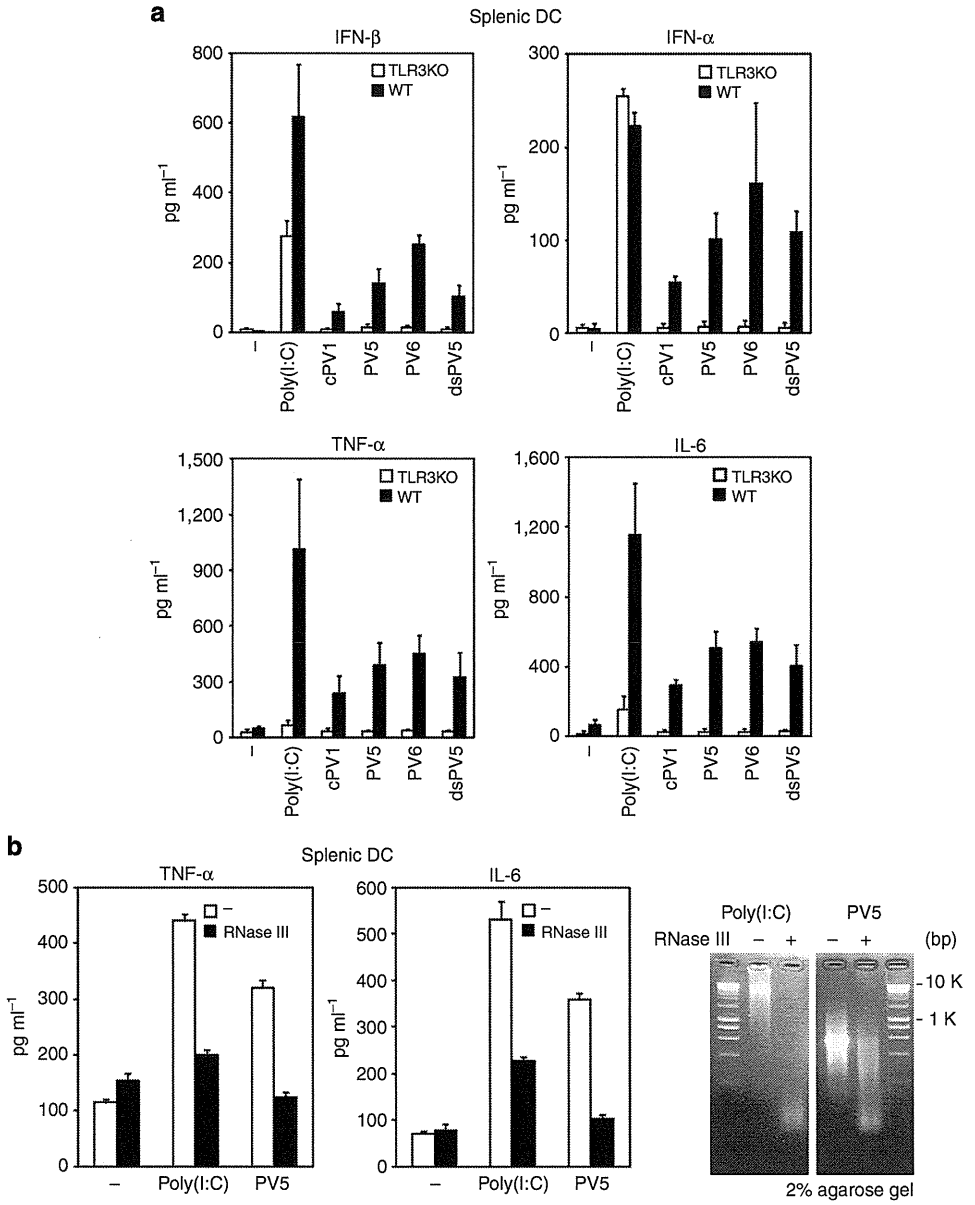

Figure 5 | Mouse splenic DCs produce type I IFN and cytokines in response to PV-RNAs in a TLR3-dependent manner. (**a**) Splenic CD11c$^+$ DCs (1×10^6 per ml) isolated from TLR3$^{-/-}$ or WT mice were stimulated with 20 μg ml^{-1} poly(I:C) or PV-derived RNAs in FCS-containing medium. Twenty-four hours after stimulation, culture supernatants were collected, and IFN-α/β in the supernatants was quantified using ELISA. TNF-α and IL-6 levels were measured using CBA. Representative data from three independent experiments are shown (mean ± s.d.). (**b**) Poly(I:C) and PV5 (20 μg ml^{-1}) were pre-treated with RNaseIII for 30 min at 37 °C or left untreated before adding to CD11$^+$ splenic DCs (1×10^6 per ml) isolated from WT mice. Twenty-four hours after stimulation, TNF-α and IL-6 levels were measured in culture supernatants using CBA (left panels). RNaseIII-treated poly(I:C) and PV5 were electrophoresed on a 2% agarose gel (right panels).

failed to induce TLR3-mediated IFN-β promoter activation by either extracellular stimulation in FCS-free medium or direct endosomal delivery using DOTAP (Fig. 7b,c). When PV5-D2 and -D4 were added to mouse splenic DCs or bone marrow-derived macrophages in the FCS-free conditions, IFN-β and proinflammatory cytokines, including TNF-α and IL-6, were produced in a TLR3-dependent manner, though their levels were relatively low compared with those induced by PV5-D1, D3 or D5 (Fig. 7d). These results suggest that longer stem structure with bulge and internal loops typically shown in PV5-D5 mfold model is the core RNA structure required for TLR3 activation in PV5 and also in PV6. In addition, shorter mismatched RNA duplexes such as PV5-D2 and -D4 can be recognized by TLR3 with less activity in mouse DCs/macrophages if they hold the structure, which differs from TLR3 response in HEK293 cells. Given that RNA molecules have an appropriate tertiary interactions, the stability and TLR3-binding ability of these RNA molecules must be influenced by RNA tertiary structure.

Discussion

In the current study, we demonstrated, for the first time, that mouse/human TLR3 detects extracellular virus-derived RNA with stable stem structures to induce innate immune signalling. Functional PV-RNAs were degradation-resistant, and their ability